Experimental Reports

(2016)

Activity Report on Neutron Scattering Research: Experimental Reports Vol. 22 (2016)

Published by:
Neutron Science Laboratory,
Institute for Solid State Physics,
University of Tokyo
106-1, Shirakata, Tokai,
Ibaraki 319-1106,
JAPAN

This volume contains experimental reports submitted in the following period of time: 2016/06/21 to 2017/06/21.
Visit our on-line database for updated information.

Structures and Excitations

Magnetism

Activity Report on Neutron Scattering Research: Experimental Reports **22** (2016) Report Number: 1734

- The investigation on the ground state of paramagnetic Cu3(P2O6OD)2 using neutron diffraction in magnetic fields
  M. Hase, V. Pomjakushin and A. Doenni
  Activity Report on Neutron Scattering Research: Experimental Reports **22** (2016) Report Number: 1739

- Magnetic structure of multiferroics CeFe3(BO3)4
  Shohei Hayashida, Daiki Kato, Takatsugu Masuda
  Activity Report on Neutron Scattering Research: Experimental Reports **22** (2016) Report Number: 1755

- Magnetic Diffuse Scattering of LuBaCo4O7 with kagome and triangular lattices
  M. Soda, M. Hagihala, and T. Masuda
  Activity Report on Neutron Scattering Research: Experimental Reports **22** (2016) Report Number: 1775

- Magnetic Excitation in Oxygen Molecule Adsorbed in Nanoporous Metal Complex Cu2(4-F-bza)4(2-mpyz)
  Takatsugu Masuda, Minoru Soda, Shinichiro Asai
  Activity Report on Neutron Scattering Research: Experimental Reports **22** (2016) Report Number: 1777

- Large magnetic anisotropy induced by high-pressure torsion straining
  N. Adachi, Y. Oba, Y. Todaka
  Activity Report on Neutron Scattering Research: Experimental Reports **22** (2016) Report Number: 1785

- Investigation on magnetic devil's staircase in La5Mo4O16
  Kazuki Iida, Ryoichi Kajimoto, Masaaki Matsuda, and Feng Ye
  Activity Report on Neutron Scattering Research: Experimental Reports **22** (2016) Report Number: 1786

- Low-energy magnetic excitations in YIG
  Y. Nambu, Y. Okino, S. Yano, and J.S. Gardner
  Activity Report on Neutron Scattering Research: Experimental Reports **22** (2016) Report Number: 1788

- Polarized neutron scattering investigation of the spin wave excitations in YIG
  Y. Nambu, Y. Okino, T. Kikkawa, K. Kakurai, B. Winn, and J. Tranquada
  Activity Report on Neutron Scattering Research: Experimental Reports **22** (2016) Report Number: 1794

- Antiferromagnetic state of Heusler alloy Ru2CrSi
  I. Shigeta, M. Hagihala, K. Fuchizaki, M. Hiroi, Y. Nambu
  Activity Report on Neutron Scattering Research: Experimental Reports **22** (2016) Report Number: 1797

- Uniaxial pressure effect on magnetic ordering in a frustrated isosceles triangular lattice Ising antiferromagnet CoNb2O6
  Setsuo Mitsuda, Ryuta Henmi, Takahiro Shimizu
  Activity Report on Neutron Scattering Research: Experimental Reports **22** (2016) Report Number: 1802

- Determination of the magnetic structure of the spin-1/2 tetramer compound CuInVO5
  Hase M., Ebukuro Y., Kuroe H., and Hester J.

Activity Report on Neutron Scattering Research: Experimental Reports **22** (2016) Report Number: 1807

- Magnetic structure of the magnetic field induced phase in non-centrosymmetric Pr5Ru3Al2
  K. Makino, D. Okuyama, T. Hong, T. J. Sato
  Activity Report on Neutron Scattering Research: Experimental Reports **22** (2016) Report Number: 1809

Strongly Correlated Electron Systems

- Evidence for f-electron multipole ordered phase of PrIr2Zn20
  K. Iwasa, T. Onimaru, K. T. Matsumoto, T. Takabatake, J.-M. Mignot, A. Goukasov
  Activity Report on Neutron Scattering Research: Experimental Reports **22** (2016) Report Number: 1711

- Uniaxial-pressure control of ferroelectricity in a spin-driven magneto-electric multiferroic CuFeO2
  Hiromu Tamatsukuri, Setsuo Mitsuda, Ryuta Henmi
  Activity Report on Neutron Scattering Research: Experimental Reports **22** (2016) Report Number: 1718

- Small angle neutron scattering on Sr2RuO4
  H.Furukawa
  Activity Report on Neutron Scattering Research: Experimental Reports **22** (2016) Report Number: 1746

- Vortex study on Fe-based superconductors
  H.Furukawa
  Activity Report on Neutron Scattering Research: Experimental Reports **22** (2016) Report Number: 1747

- Weak ferromagnetic superconductor Tb0.47Y0.53Ni2B2C
  Misato Takahashi
  Activity Report on Neutron Scattering Research: Experimental Reports **22** (2016) Report Number: 1767

- Weak ferromagnetic superconductor Tb0.47Y0.53Ni2B2C
  Misato Takahashi
  Activity Report on Neutron Scattering Research: Experimental Reports **22** (2016) Report Number: 1768

- Determination of the Magnetic Structure of the Noncentrosymmetric Heavy-Electron Metamagnet CePdSi3
  M. Yoshida, D. Ueta, T. Kobuke, H. Yoshizawa
  Activity Report on Neutron Scattering Research: Experimental Reports **22** (2016) Report Number: 1783

- Neutron spin echo measurements on the iron-based ladder compound BaFe2Se3
  Y. Nambu, M. Nagao
  Activity Report on Neutron Scattering Research: Experimental Reports **22** (2016) Report Number: 1795

- Domain Formation and Ground State of Spin and Charge Order for RFe2O4 (R=Yb and Lu)
  Kosuke Fujiwara, Yohei Okuda, Tomoyuki Karasudani, Naoshi Ikeda, Kazuhisa Kakurai
  Activity Report on Neutron Scattering Research: Experimental Reports **22** (2016) Report Number: 1805

Biology

- Subunit exchange study on alpha-crystallin hetero-oligomer
  Rintaro Inoue, Masaaki Sugiyama, Nobuhiro Sato, Yojiro Oba
  Activity Report on Neutron Scattering Research: Experimental Reports **22** (2016) Report Number: 1719

Soft Matters

- Structure of imidazolium-based ionic liquid under shear flow
  F. Nemoto, M. Nagao, K. Weigandt, H. Seto, Y. Kitazawa, M. Hirasawa, T. Ueki, M. Watanabe
  Activity Report on Neutron Scattering Research: Experimental Reports **22** (2016) Report Number: 1736

- Structural study on the "nonswellable" hydrogel
  S. Nakagawa, X. Li, and M. Shibayama
  Activity Report on Neutron Scattering Research: Experimental Reports **22** (2016) Report Number: 1753

- Structure of Polyelectrolytes under Electric Field
  Xiang Li, Mitsuhiro Shibayama
  Activity Report on Neutron Scattering Research: Experimental Reports **22** (2016) Report Number: 1778

- Aggregation structure of thermoresponsive hydrogels consisting of a homogeneous network
  S. Nakagawa, X. Li, and M. Shibayama
  Activity Report on Neutron Scattering Research: Experimental Reports **22** (2016) Report Number: 1787

- Elucidation of the Mechanism of the Solvent-Dependent Switch of Helical Main-Chain Chirality of Poly(quinoxaline-2,3-diyl)s by Small Angle Neutron Scattering
  Yuuya Nagata, Sota Sato, Masaaki Sugiyama
  Activity Report on Neutron Scattering Research: Experimental Reports **22** (2016) Report Number: 1796

- Thermodynamical Study on Phase Behavior of Thermo-responsive Polymer in Hydrophobic Ionic Liquids.
  Kazu Hirosawa, Xiang Li, Ken Morishima, and Mitsuhiro Shibayama
  Activity Report on Neutron Scattering Research: Experimental Reports **22** (2016) Report Number: 1801

Others

- Investigation of nanoparticles in ODS Ni-free austenitic steel
  A. Kowalska-Mori,
  Activity Report on Neutron Scattering Research: Experimental Reports **22** (2016) Report Number: 1770

Structures and Excitations

Investigation of the magnetic ground state in a new one-dimensional quantum spin system K2Cu3O(SO4)3

Masayoshi Fujihara, Setsuo Mitsuda and Shinichiro Yano2
Department of Physics, Faculty of Science, Tokyo University of Science, Tokyo 162-8601, Japan,
2 National Synchrotron Radiation Research Center, Neutron Group, Hsinchu 30077, Taiwan

For discovery of a exotic ground states, we tried to synthesize a new quantum spin system K2Cu3O(SO4)3 and finally succeeded in preparing pure-phase. The magnetic ions of Cu2+ form edge-sharing spin tetrahedral cluster and that are connected each other by SO42- ions along the b-axis direction. The inter-cluster magnetic interactions should be weaker than intra-cluster magnetic interactions because it is next-nearest-neighbor magnetic interaction through the Cu-O-S-O-Cu exchange paths, so we called this system " the edge-sharing tetrahedral cluster chain system ". The competing of the edge-sharing tetrahedral frustration and one-dimensionally weak inter-tetrahedra magnetic couplings are expected in this unique structure of K2Cu3O(SO4)3.

Short-range magnetic correlations were observed to develop in two-stage process at around 100 K and 4 K without long-range ordering. Magnetization datas showed the 1/3 plateau both above and below 4K. We observed only a Schottky-like anomaly at around 5 K and any anomaly indicative of long-range ordering is absent down to at least 0.5 K in the specific heat.

The inelastic neutron scattering (INS) on powder K2Cu3O(SO4)3 was performed on a cold-neutron time-of-flight chopper spectrometer, PELICAN installed at ANSTO. In Fig.1 (a), a data of T = 1.6 K, the dispersive excitation and a gap of $\Delta \sim 0.8$ meV was observed definitely, which shows the characteristic of the one dimensional spin gap system. In Fig.1 (b), a data of T = 20 K, the gapless dispersive excitation is observed, indicating the development of one dimensional short range correlations.

These experimental results is explained theoretically as follows. Three spin-triplet state which formed in a cluster in spite of the antiferromagnetic interactions are dominant, and which can be described the composite Haldane spin chains.

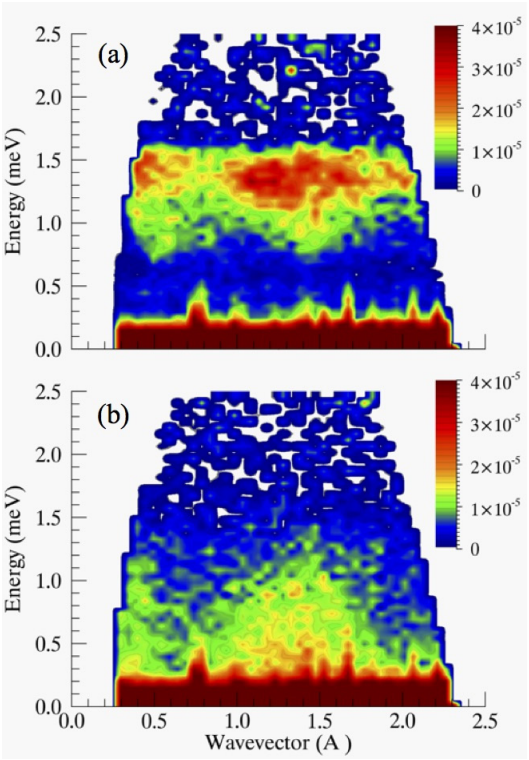

Fig. 1. Inelastic neutron spectra measured at (a) 1.6 K and (b) 20 K. The incident neutron wavelength was 4.75 A.

Magnetic correlations in spin-3/2 perfect kagome Li2Cr3SbO8

Kazuki Iida, Hiroyuki Yoshida, Shinichiro Yano, and Richard Mole
CROSS, Hokkaido University, and ANSTO

Network of corner sharing triangles forms kagome lattice. When the antiferromagnetic nearest-neighbor (NN) interaction exists the system shows geometrical frustration. Due to the geometrical frustration, classical kagome lattice Heisenberg antiferromagnet (CKLHAF) has infinitely degenerated ground states which are connected by zero-energy modes. Order by disorder theory predicted that quantum fluctuation favors so-called $\sqrt{3} \times \sqrt{3}$ order at $T \rightarrow 0$ among the many possible states. Experimentally, the magnetic long range order with a $\mathbf{q} = 0$ structure which has different spin chirality from that of the $\sqrt{3} \times \sqrt{3}$ structure was reported in several CKLHAF materials such as Cr and Fe jarosites. This is because Dzyloshinsky-Moriya (DM) interaction and/or single-ion anisotropy lead to $\mathbf{q} = 0$ structure. Therefore, experimental realization of $\sqrt{3} \times \sqrt{3}$ short-range order or classical spin-liquid ground state is highly desirable to understand the nature of the CKLHAF model.

Recently, CKLHAF material, $Li_2Cr_3SbO_8$ was synthesized. $Li_2Cr_3SbO_8$ has a $P6_3mc$ space group (No186, hexagonal), where magnetic Cr^{3+} ions (t_{2g}^3, $S = 3/2$) locate at $6c$ site [$(x, -x, z)$ with $x = 1/6$ and $z = 0.2478$] and form a "perfect" kagome lattice. Since there are nonmagnetic Li^+ and Sb^{5+} layers between kagome layers, the kagome planes have good two-dimensional feature. In spite of the large negative Curie-Weiss temperature $\Theta_{CW} = -541.3$ K, no long-range order was observed down to 0.1 K confirmed by μSR. There is no difference between zero field cool and field cool in magnetic susceptibility, suggesting that spin glass state is ruled out from the ground state. Furthermore, magnetization measurements indicate the negligible DM interaction. The ground state of $Li_2Cr_3SbO_8$ is considered to be classical spin liquid.

Polycrystalline $Li_2Cr_3SbO_8$ was prepared by conventional solid state reactions for neutron experiments. 8 g powder was put into the annular can. Inelastic neutron scattering experiments were done at time-of-flight (TOF) neutron spectrometer PELICAN in ANSTO. Measurements were performed at 1.5, 15, 30, 60, and 120 K with $E_i = 10.9$ meV and 1.5, 4.5, 15, and 30 K with 3.63 meV. Empty can was also measured for both E_i, which was subtracted from the raw data. Vanadium was also measured for correction.

Fig. 1(a) shows neutron diffraction patterns with the energy window of $\hbar\omega = [-0.25, 0.25]$ meV at 1.5 and 15 K using $E_i = 10.9$ meV. Broad peaks was observed at $Q \sim 0.7$ and 1.4 Å^{-1}, corresponding to $(1/3, 1/3, 0)$ and $(2/3, 2/3, 0)$ positions, respectively. The broad peaks suggest the existence of short-range correlations. Fig. 1(b) shows inelastic neutron scattering map in $Li_2Cr_3SbO_8$ at $T = 1.5$ K with $E_i = 10.9$ meV. Quasielastic magnetic excitation centered at $Q = 1.3$ Å^{-1} was observed up to about 4 meV. Furthermore, additional magnetic excitation at $\hbar\omega = 7$ meV was also observed. To discuss the nature of the low-energy magnetic excitation, Q dependence of the magnetic excitations at $\hbar\omega = [1, 3]$ meV at 1.5 K is plotted in Fig. 1(c). The Q dependence can be well reproduced by the simulation assuming the 3×3 short-range magnetic order. This feature suggests that low-energy magnetic excitations observed in $Li_2Cr_3SbO_8$ originate in the classical spin liquid feature of $Li_2Cr_3SbO_8$. Interestingly, the maximum intensity of the Q dependence shifts to lower Q with increasing temperature (120 K), which is a common feature of the "quantum spin liquid" systems such

as spin-1/2 kagome $ZnCu_3(OD)_6Cl_2$ and spin-1/2 triangular $YbMgGaO_4$. Note that peaks positions at $Q = 2.8$ and 3.6 $Å^{-1}$ correspond to the nuclear Bragg peaks, suggesting that these peaks are phonon. On the other hand, Q dependences of the magnetic excitations at $\hbar\omega = [6.5, 8.5]$ meV at 1.5 and 120 K are also plotted in Fig. 1(d). These Q dependences cannot be explained by simple magnetic form factor of Cr^{3+} ions and we need to add another component from the classical spin liquid, indicating that the higher energy mode originates in combination of the crystal field and classical spin liquid. The energy dependences of the classical spin liquid excitation at $Q = [1, 1.8]$ $Å^{-1}$ are also plotted in Fig. 1(e). Surprisingly, the energy spectrum at 1.5 K shows the spin gap which disappear above 15 K. Using the relationship, $\chi''(\hbar\omega) = I(\hbar\omega)(1 - e^{-\hbar\omega/k_BT})$, we also obtained the imaginary part of dynamical susceptibility $\chi''(\hbar\omega)$. Finally, we plotted the scaling plot ($\chi''(\omega)T$ vs ω/T) in Fig. 1(f). The experimental data well fitted by $\chi''(\hbar\omega)k_BT^{\alpha} \propto (k_BT/\hbar\omega)^{\alpha}\, tanh\,(\hbar\omega/\beta k_BT)$ with $\alpha = 0.840(1)$ and $\beta = 1.118(8)$.

Since $Li_2Cr_3SbO_8$ is the only material whose ground state is the classical spin liquid among the CKLHAF systems, we believe that our findings on the magnetic excitations in $Li_2Cr_3SbO_8$ can shed light on the classical spin liquid state.

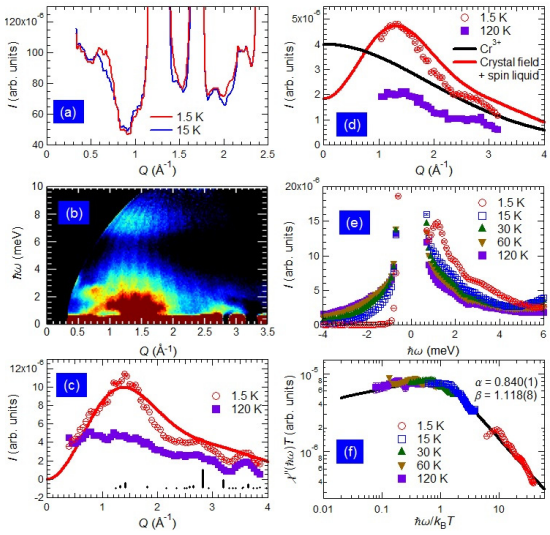

Fig. 1. (a) Neutron diffraction patterns. (b) Inelastic neutron scattering map. (c) Q dependences at 2 meV. (d) Q dependences at 7.5 meV. (e) Energy dependences at 1.4 $Å^{-1}$. (f) Scaling plot.

Structural investigation about new perovskite related AA'BO4 structure of oxide-ion conductors

W. Uno, K. Fujii, M. Yashima
Tokyo Institute of Technology

To investigate the crystal structure of various metal oxides, I conducted the neutron powder diffraction at ECHIDNA, ANSTO. As I refined the diffraction data measured in this time, atomic arrangement of the substance became clear. I understood the mechanism of oxide ion diffusion path in the structure.

Spin dynamics of quantum spin liquid state in kapelasite

Kazuki Iida, Hiroyuki Yoshida, Motoyuki Ishikado, Masaaki Matsuda, and Gabriele Sala
CROSS, Hokkaido University, and ORNL

Ground state of the spin-1/2 perfect kagome lattice is believed to be a quantum spin liquid (QSL) state. It is of great interest whether or not intrinsic spin gap exists in the QSL state [S. Yan *et al*., Science **332**, 1173 (2011).], which gives us strong constrain to construct the QSL theory. So far, all reported spin-1/2 perfect kagome-lattice compounds have impurity (i.e., atomic intersite randomness between Cu^{2+} and nonmagnetic ions), which prevents us to investigate the existence of spin gap because impurity gives rise to low-energy scattering [T.-H. Han *et al*., PRB **94**, 201111 (2016).]. To discuss the spin gap problem in the spin-1/2 perfect kagome lattice, we performed single-crystal inelastic neutron scattering measurements on newly discovered spin-1/2 perfect kagome compound $CaCu_3(OH)_6Cl_2{\cdot}0.6H_2O$.

Recently, we have succeeded in growing large single crystals of the new kagome material, $CaCu_3(OH)_6Cl_2{\cdot}0.6H_2O$ [H. Yoshida *et al*., submitted]. By means of single-crystal X-ray diffraction measurements, we determined its crystal structure. $CaCu_3(OH)_6Cl_2{\cdot}0.6H_2O$ has the $P3m1$ space group (No156, trigonal), and magnetic Cu^{2+} ions with $S = 1/2$ form a perfect kagome lattice. We address that Ca^{2+}/Cu^{2+} intersite disorder was " not " observed in our single crystal X-ray diffraction measurement because of the large difference between their ionic radii. No signature of magnetic long-range order or spin glass was observed in magnetic susceptibility and μSR measurements down to 0.1 K. Currie-Weiss fit gives S = 1/2 and $\Theta_{CW} = -60$ K, indicating antiferromagnetic interactions. In heat capacity measurement, T-linear term ($\gamma = 10.2$ mJ/Cu mol K^2) was observed, suggesting that the ground state is QSL. Therefore, $CaCu_3(OH)_6Cl_2{\cdot}0.6H_2O$ is an ideal compound to investigate the spin gap problem in the spin-1/2 perfect kagome-lattice antiferromagnet.

Very recently, we measured inelastic neutron scattering (INS) on powder $CaCu_3(OD)_6Cl_2{\cdot}0.6D_2O$ at the cold-neutron chopper spectrometer LET in ISIS. Clear spin gap of 0.78(2) meV was observed at 0.15 K. To investigate in detail the momentum vector dependence of the spin dynamics as well as the spin gap in $CaCu_3(OD)_6Cl_2{\cdot}0.6D_2O$, single crystal INS measurements are necessary. We therefore performed single-crystal INS measurements on the QSL state in $CaCu_3(OH)_6Cl_2{\cdot}0.6H_2O$ using the time-of-flight (TOF) chopper spectrometer CNCS in SNS. About four hundreds of single-crystal $CaCu_3(OH)_6Cl_2{\cdot}0.6H_2O$ with total mass of $\sim$ 2 g were co-aligned [Fig. 1(a)]. TOF measurements were performed at 1.5 and 50 K with $E_i = 12$ meV. We rotate crystals by 225° to observe the whole picture of magnetic excitations.

Figure 1(b) shows neutron diffraction pattern at 1.5 K. No magnetic excitation was observed, indicating the absence of symmetry-breaking magnetic long-range order. Figure 1(c)–1(f) show constant-energy maps. Hexagonal-shaped excitation, which is typical magnetic excitation in the kagome QSL state, was observed at 1.5 K above 1 meV. Similar magnetic excitation survives at least 8.5 meV, which can be also seen in the powder results. In the meanwhile, no hexagonal-shaped magnetic excitation was observed below 1 meV. These results indicate that spin gap with about 0.5 meV exists at 1.5 K. Therefore, we have succeeded observing the spin gap in quantum spin liquid kagome $CaCu_3(OH)_6Cl_2{\cdot}0.6H_2O$. The size of the spin gap is consistent with the powder re-

sult.

Since $CaCu_3(OH)_6Cl_2{\cdot}0.6H_2O$ is the most clean system to investigate QSL, we believe that our findings on the spin gap in $CaCu_3(OH)_6Cl_2{\cdot}0.6H_2O$ can shed light on QSL and encourage further theoretical works.

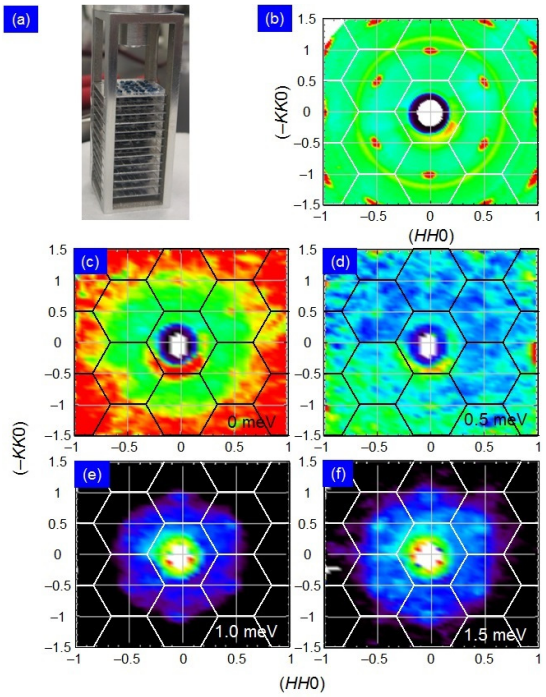

Fig. 1. (a) Picture of co-aligned single crystals. (b) Neutron diffraction pattern at 1.5 K. Constant-energy maps by subtracting the high temperature data (50 K) from the low temperature data (1.5 K) at (c) 0, (d) 0.5, (e) 1, and (f) 1.5 meV.

Crystal structure analysis of high temperature neutron diffraction data of novel oxide-ion conducting materials

Kotaro Fujii, Ayaka Fujimoto, Wataru Uno, Keigo Nakamura, Masatomo Yashima
Tokyo Institute of Technology

Oxide-ion conductors, which include pure ionic conductors and mixed oxide-ion and electronic conductors, attract significant interest because of their varied uses in oxygen separation membranes and cathodes for solid-oxide fuel cells (SOFCs). The oxide-ion conductivity is strongly dependent on the crystal structure. At present, several structures, such as fluorites, perovskites, K_2NiF_4, mellilites, and apatites, are known to show high oxide-ion conductivities. For further development of oxide-ion conductors is investigating materials with new types of structures. According to such background, we are exploring new structure family of oxide-ion conductors. For example, we have discovered a new structural family of oxide-ion conductor $NdBaInO_4$ which has a monoclinic $P2_1/c$ perovskite-related phase with a layered structure, in 2014. More recently, we found novel material, $SrRInO_4$ (R : rare earths) with $CaFe_2O_4$-type structure showed high oxide-ion conductivity compared to the other $CaFe_2O_4$-type materials. In order to understand the mechanism of oxide-ion conduction, it is necessary to precisely determine the crystal structure (particularly position, occupancy factor, and anisotropic displacement parameters of oxygens) at high-temperature because oxide-ion conductors are generally used at high-temperature. In the present study, we investigated the crystal structure of $SrRInO_4$ (R : rare earths) at high temperature using high resolution neutron powder diffractometer Echidna installed at the research reactor OPAL, ACNS, ANSTO. The materials were prepared by the solid-state reactions. The sintered pellets of the reaction products were introduced into a vanadium can and used for the neutron diffraction experiment. The measurements were carried out from room temperature to high temperature (1000 °C) at 200 °C intervals. Each measurement time was few hours. The structural analyses for these data are carried out by Rietveld method using the program RIETAN-FP. The result of the Rietveld refinement at the room temperature 23 °C is shown in Figure (R_{wp} =3.78 %, R_B = 3.82 %). For the diffraction data at 800 °C, the final Rietveld plot gave R_{wp} = 5.45 %, R_B = 6.35 % (see Figure for the fitting). Currently further structure analysis is ongoing.

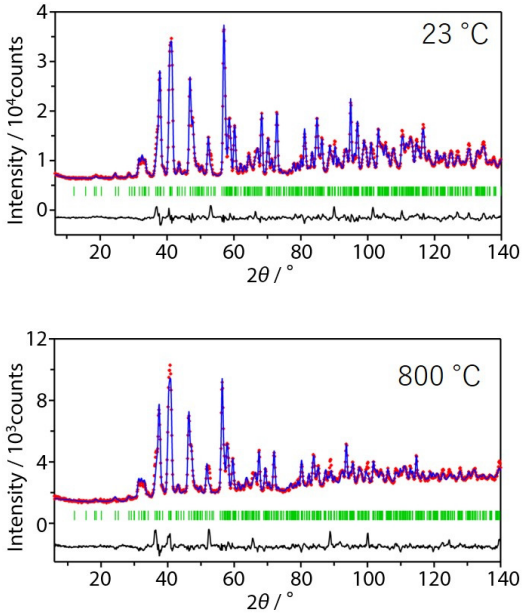

Fig. 1. Rietveld plots of SrRInO4 based material

High temperature neutron diffraction study of oxide-ion conductors

Kotaro Fujii, Keisuke Hibino, Wataru Uno, Masatomo Yashima
Tokyo Institute of Technology

Oxide-ion conductors attract significant interest because of their varied uses in oxygen separation membranes and cathodes for solid-oxide fuel cells (SOFCs). Investigation of mechanism of oxide-ion conduction will lead further development of SOFCs. In order to understand the mechanism of oxide-ion conduction, it is necessary to precisely determine the crystal structure (particularly position, occupancy factor, and anisotropic displacement parameters of oxygens) at high-temperature because oxide-ion conductors are generally used at high-temperature. Furthermore, combinations of high-temperature neutron diffraction data and maximum entropy method (MEM) can lead direct observation of ion diffusion pathway. In this context, we plan to carry out high-temperature and high-resolution neutron powder diffraction experiments for the oxide-ion conductors. There are several oxide-ion conductors for which the mechanism of the oxide-ion conduction is not clearly understood. In this study, we have investigated the crystal structure of oxide-ion conductor $A_2B_2O_7$ (A : rare earths, B : group 4 transition metal) at high temperature using high resolution neutron powder diffractometer Echidna installed at the research reactor OPAL, ACNS, ANSTO. The materials were prepared by the solid-state reactions. The sintered pellets of the reaction products were introduced into a vanadium can and used for the neutron diffraction experiment. The measurements were carried out from room temperature to high temperature (maximum 1400 °C) at 200 °C intervals. Each measurement time was few hours. The structural analyses for these data are carried out by Rietveld method using the program RIETAN-FP. The result of the Rietveld refinement at the room temperature 23 °C is shown in Figure (R_{wp} = 5.46 %, R_B = 1.72 %). For the diffraction data at 1400 °C, the final Rietveld plot is shown in Figure. The reliability factors are R_{wp} = 5.22 %, R_B = 5.80 %. There was no structure transition by heating up to 1400 °C. Now we carry out further structure analysis and MEM calculations for the data in order to the mechanism of the oxide-ion conduction in this material.

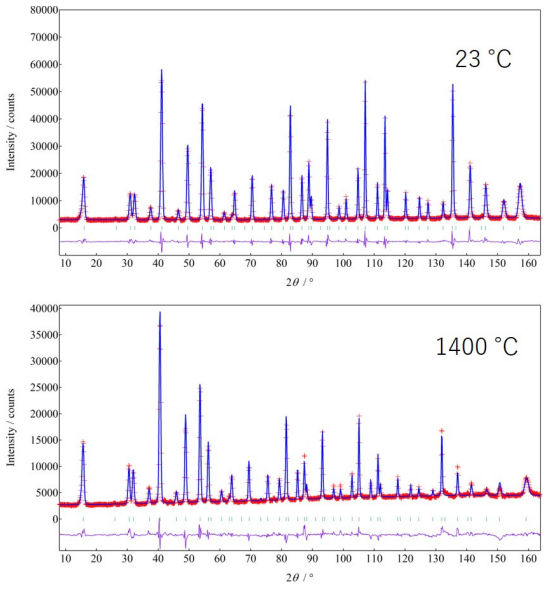

Fig. 1. Rietveld plots of A2B2O7 material

Magnetism

Neutron powder diffraction study on new square-lattice antiferromagnets Sr2CrO3X (X = F and Cl)

Yoshihiro Tsujimoto, Shinichiro Asai, Maxim Avdeev, Takatsugu Masuda, Kazunari Yamaura
NIMS, ISSP, ANSTO

Development of the understanding of the transition metal oxides has triggered the search for hetero-anion containing metal oxides because incorporation of hetero anions which possess different charge, electronegativity, and ionic size from the oxide ion opens up possibilities for inducing new physical and chemical properties that the corresponding pure oxide does not exhibit. Recently, we have demonstrated that controlling mixed-anion site ordered patterns is a new effective approach to drastically switch the magnetic/electronic ground states [1]. For example, Sr2NiO3X (X = F, Cl) with the low spin state (S = 1/2) adopts the K2NiF4 type structure, but the nickel cation takes a square pyramidal coordination with apical O/X anions being ordered for X = Cl and disordered for F (Fig. 1a). Each square pyramid NiO5 is linked by corner sharing so as to form a two-dimensional square lattice. In contrast to related layered compounds such as K2NiF4 and La2CuO4 having the strong superexchange interactions through dx2?y2 and O2p orbitals, the half-filled dxy orbital in Sr2NiO3X gives rise to sizable direct (FM) interactions along the diagonal direction on a square, the magnitude of which depends on the direction of Ni-centered square pyramids (or the O/X site ordered patterns). As a result, X = Cl undergoes an AFM ordering at TN = 47 K, and a spin disordered state below 11 K for X = F.

In order to develop our approach, we synthesized new chromium oxyhalide compounds, Sr2CrO3X (X = F, Cl) with (t2g)3 orbitals, by high-pressure method, which are isostructural with Sr2NiO3X including the O/X ordered patterns. As we expected, the chromium oxyhalides exhibit greatly different magnetic susceptibility curves between them. X = F and Cl show a broad maximum at Tmax = 290 and 56 K, respectively. The magnetic phase transition temperatures, which are estimated from dX/dT, are 150 K for X = F and 27 K for X = Cl. In this study, we conducted neutron powder diffraction experiments using ECHIDNA instrument installed in ANSTO to investigate their magnetic ground state.

Figure 1c shows the temperature evolution of the neutron diffraction patterns collected from the oxyfluoride. At the base temperature, some addition peaks which could not be assigned by the chemical unit cell were clearly observed. These peaks disappeared above 150 K, and thus the origin of them should be magnetic. Rietveld refinement gave the best agreement with the propagation vector k = (1/2 1/2 0) and Cr spins aligned along the c direction. The figure 1d displays the temperature variation of the magnetic moments. They increase with decreasing temperature and the magnitude of them is approximately 2.0 ?B at 3 K. This is consistent with the trivalent chromium ion. In contrast, the neutron diffraction pattern for Sr2CrO3Cl evidenced no long-range magnetic order down to 3 K (Fig 1b). The data showed only two magnetic peaks which could be assigned to (1/2 1/2 0) and (1/2 1/2 1). No observation of (1/2 1/2 l), $l > 1$ suggests that Cr spins are antiferromagnetically correlated in a bilayer unit, but a magnetic correlation between bilayers are negligible. It is very interesting to clarify what makes the difference in the magnetic ground states of the oxychloride and oxyfluoride.

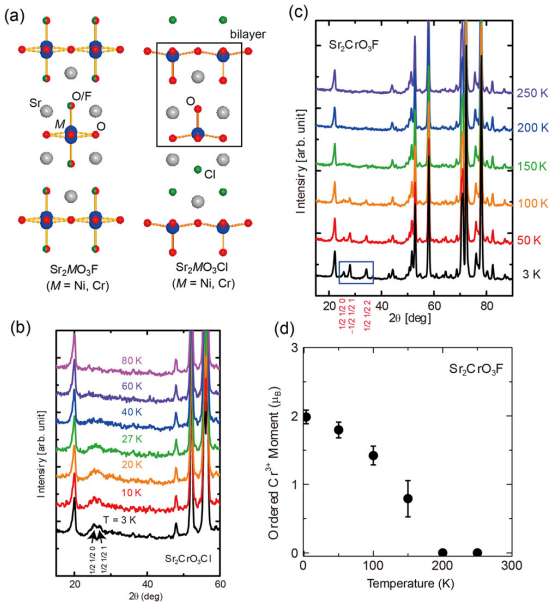

Fig. 1. Fig. 1(a) Crystal structures of Sr2MO3X (M = Ni, Cr; X = F, Cl). (b, c) Neutron diffraction patterns collected from Sr2CrO3Cl and Sr2CrO3F at various temperatures. (d) Temperature evolution of the magnetic moments of Cr3+ spin in Sr2CrO3F.

The investigation on the ground state of paramagnetic Cu3(P2O6OD)2 using neutron diffraction in magnetic fields

M. Hase1, V. Pomjakushin2 and A. Doenni1
1 NIMS, 2 PSI

We can investigate magnetism on each site even in magnets without magnetic long-range order using neutron diffraction. Magnetic moments are induced by magnetic fields and generate magnetic reflections. We can evaluate a field-induced magnetic moment (magnetization) on each site from analyses of the magnetic reflections. We succeeded in the determination of the magnetic moments on two types of Mn2+-ion sites in the antiferromagnetic (AF) trimer compound SrMn3P4O14 using the HRPT diffractometer [1].

We have paid our attention to Cu3(P2O6OD)2. No magnetic order appears down to 2 K. As shown in the inset of Fig. 1, two types of Cu2+-ion sites exist. The AF trimerized spin chain with J1 = 111 K and J2 = 30 K can explain magnetization and inelastic neutron scattering results [2,3]. The J1 interaction is dominant and forms Cu2-Cu2 AF dimers. Therefore, the field-induced magnetic moment on Cu2 sites is expected to be smaller than that on Cu1 sites.

We performed neutron diffraction experiments on pressed pellets of Cu3(P2O6OD)2 using the HRPT diffractometer with the MA6 magnet. The wavelength is 1.886 Å. The circles in Fig. 1 show a neutron diffraction pattern at 1.8 K in the zero magnetic field. We performed Rietveld refinements using P-1 to evaluate crystal structure parameters. The line on the experimental pattern indicates the result of Rietveld refinements. The line agrees well with the experimental pattern. We could determine the position of deuterium D as x = 0.2499(9), y = 0.3899(6), and z = 0.8460(5). The positions of the other atoms are close to those in the literature [4]. We observed no magnetic reflection.

Figure 2 shows neutron diffraction patterns of Cu3(P2O6OD)2 at 1.8 K and 25 K in H = 6 T. The patterns are almost the same. A small difference may exist around 14.3 °. We could not obtain field-induced magnetic moments. We will submit a proposal to perform neutron diffraction experiments using the DMC diffractometer with the MA6 magnet.

Magnetic structure of multiferroics $CeFe_3(BO_3)_4$

Shohei Hayashida, Daiki Kato, Takatsugu Masuda
ISSP The University of Tokyo

Coexistence of magnetic order and electric polarization, *multiferroicity*, has become a top major topic over the past decade in condensed matter physics. Rare-earth ferroborates $RFe_3(BO_3)_4$ (R = Y and rare-earth metal show diverse magnetoelectric (ME) effect as a function of the R^{3+} ions [1]. We succeeded in synthesizing high quality single crystal of $CeFe_3(BO_3)_4$ by a flux method. The crystal structure is a trigonal and the space group is $R32$. Although Hinatsu *et al*. reported that a magnetic long range order appeared at $T_N = 29$ K from specific heat and magnetic susceptibility of polycrystalline sample [2], there is no other report on $CeFe_3(BO_3)_4$. In order to investigate the multiferrocity of $CeFe_3(BO_3)_4$, it is very important to identify the magnetic structure.

We performed neutron diffraction experiment to identify the magnetic structures of the compound. The polycrystalline sample was prepared by a flux method. The mass of the samples was 2.9 g. ECHIDNA diffractometer was used. Ge 331 monochromator was chosen to obtain the neutrons with the wave length of 2.4395 Å. A closed cycle refrigerator was used to achieve 3.7 K as a base temperature. Figure 1(a) shows the diffraction profiles at 3.7 K and 50 K. The nuclear reflection profile is consistent with the crystal structure previously reported. More than 10 additional peaks are observed below 30 K. The intensities of these peaks increase with decrease of the temperature, meaning that they are magnetic Bragg peaks. Figure 1(b) shows the temperature dependence of the diffraction patterns around $2\theta = 27.5°$. There are three magnetic Bragg peaks at $2\theta = 26.8°$, $27.7°$ and $28.5°$ in $T = 3.7$ K. The positions of the peaks at $2\theta = 26.8°$ and $28.5°$ shift to $27.7°$ with increase of the temperature.

The peak at $2\theta = 27.7°$ is indexed by a propagation vector $\boldsymbol{k}_1 = (0, 0, 1.5)$. The peaks at $2\theta = 26.8°$ and $28.5°$ are incommensurate peaks and indexed by a propagation vector $\boldsymbol{k}_2 = (0, 0, 1.5 + \varepsilon)$, where value of ε is 0.046 at $T = 3.7$ K and decrease with increase of the temperature. Analyzing the magnetic structure using Rietveld refinement, it is found that the magnetic moments of the Ce^{3+} adn Fe^{3+} ions are aligned in the crystallographic ab-plane and antiferromagnetically propagate along the c-axis with $\boldsymbol{k}_1 = (0, 0, 1.5)$. On the other hand, the magnetic moments with $\boldsymbol{k}_2 = (0, 0, 1.5 + \varepsilon)$ construct a proper screw structure along the c-axis. The periodicity of the proper screw structure becomes long with increase of the temperature since the ε decreases with increase of the temperature. The detailed analysis of the magnetic structure is now in progress.

References

[1] A. M. Kadomtseva *et al*., Low Temp. Phys. **36**, 511 (2010).
[2] Y. Hinatsu *et al*., J. Solid State Chem. **172**, 438 (2003).

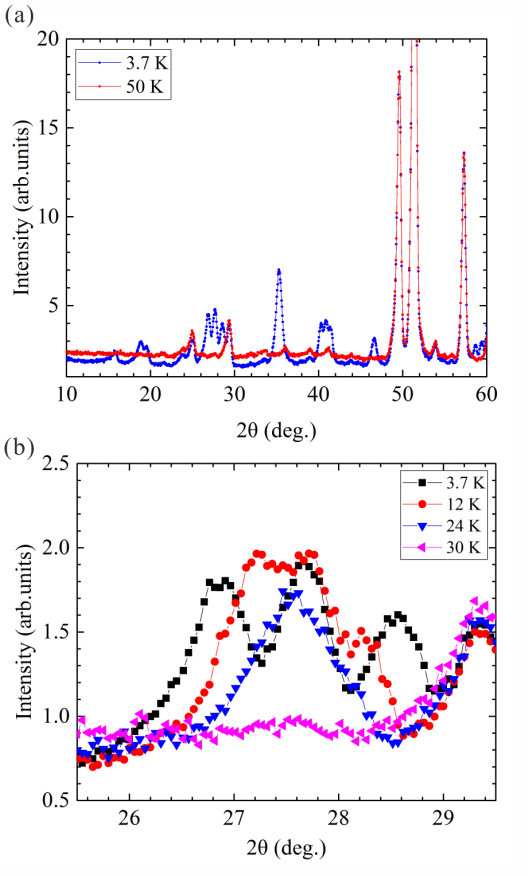

Fig. 1. (a) Neutron diffraction profiles at $T = 3.7$ K and 50 K. (b) A temperature dependence of the diffraction patterns around $2\theta = 27.5°$.

Magnetic Diffuse Scattering of LuBaCo4O7 with kagome and triangular lattices

M. Soda, M. Hagihala, and T. Masuda
Neutron Science Laboratory, Institute for Solid State Physics, University of Tokyo, Tokai, Ibaraki 319-1106, Japan

Spin systems on the pyrochlore, triangular and kagome lattices are well-known examples of geometrically frustrated systems and expected to exhibit various interesting properties induced by strong magnetic fluctuations. RBaCo4O7 (R=Ca, Y, and rare-earth elements) is one of typical examples of such systems, because it has both triangular and kagome lattices formed by CoO4 tetrahedra.

Previously we have carried out the neutron scattering measurement on the single crystals of YBaCo4O7[1] and LuBaCo4O7[2]. In the study of YBaCo4O7, the magnetic transitions were found at two temperatures 70 and 105 K. At 10 K, superlattice reflections were observed at the Q-points (h/2,k/2,0) and (h/3,k/3,0). At 110 K, the line-shape-diffuse scattering connecting (h/2,k/2,0) and (h/3,k/3,0) was observed. The line-shape-diffuse scattering has the maximum intensity at around 105 K, and the superlattice reflections and the line-shape-diffuse scattering coexist below 105 K. The temperature dependence of the line-shape-diffuse scattering connecting the magnetic Bragg points indicates the possibility of the Z2 vortex (topological) transition which is characterized by its parity.[3]

In the isostructural LuBaCo4O7, the magnetic transition has been observed at 105 K. In order to clarify the existence of Z2 vortex order, we measured the detailed temperature dependence and the shape of the magnetic diffuse scattering in LuBaCo4O7 by using CORELLI installed at SNS.

Figures 1(a) and 1(b) show the neutron intensity measured at 6 K for Q=(H,K,0) and Q=(H,K,2), respectively. The characteristic diffuse scattering and the superlattice reflections were obserbed at low temperature. With increasing temperature, the intensities of the line-shape-diffuse scattering and the superlattice reflections decrease. The line-shape-diffuse scattering in LuBaCo4O7 has the maximum intensity at the low temperature. The temperature dependence of the line-shape-diffuse scattering in LuBaCo4O7 is different from that in YBaCo4O7. At this moment, we try to analyse the neutron results of both LuBaCo4O7 and YBaCo4O7 in consideration of the Z2-vortex transition.

References

[1] M. Soda, et al., JPSJ. 75, 054707 (2006) and M. Soda, et al.,in preparation
[2] M. Soda, et al., JPSJ. 76, 084701 (2007).
[3] T. Okubo and H. Kawamura, JPSJ. 79, 084706 (2010).

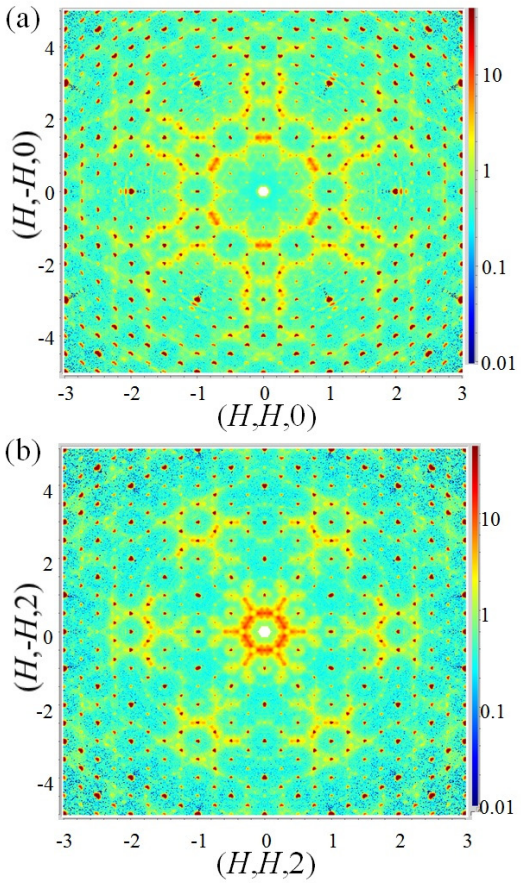

Fig. 1. Elastic neutron intensities measured at 6 K for (a) Q=(H,K,0) and (b) Q=(H,K,2).

Magnetic Excitation in Oxygen Molecule Adsorbed in Nanoporous Metal Complex Cu2(4-F-bza)4(2-mpyz)

Takatsugu Masuda, Minoru Soda, Shinichiro Asai
Institute for Solid State Physics, the University of Tokyo

In some types of nanoporous metal organic complex, gas molecules are adsorbed in the porous, leading to realization of supercrystal of the molecules. One of the most interesting examples is a Cu complex, CPL-1, that adsorbs O2 molecule, S = 1 magnetic entity, in its one dimensional cylindrical porous [1]. The O2 molecules form ladder like structure and S = 1 spin gap system was expected. The neutron spectrum at low temperature was explained by the singlet-triplet excitation of S = 1 dimer [2]. Meanwhile the temperature dependence deviates from the dimer model. Combination of calculation on spin-dependent molecular potential [3] and neutron scattering results indicated that the origin of the unconventional dynamics was the soft framework of oxygen supercrystal. In this studies, unfortunately, protonated samples were used, and the signal to noise ratio was not good, leading to difficulty in the precise measurement on weak intensities, particularly at higher temperatures.

A Cu complex, Cu2(4-F-bza)4(2-mpyz), is a new nanoporous material. The adsorbed O2 molecules form trimer structure in its nanopore [4]. M-H curve at 2 K is reasonably explained by antiferromagnetic S=1 trimer model with intratrimer interaction J = -20 K and single-ion anisotropy D = 2.1 K. In contrast to the magnetization, the temperature dependence of the susceptibility is not reproduced by the trimer model indicated by solid curve. This suggests that the higher energy scheme is not explained by conventional spin system. We performed a neutron scattering experiment using chopper spectrometer to obtain overall spectrum of the supercrystal of O2 molecules.

Neutron scattering experiment was performed on cold-neutron TOF spectrometer PELICAN at ANSTO. We used cryogen-free cryostat for achieving low temperature. We used 1.2 g of deuterated sample. We chose the incident neutron energy of 2.2, 3.7, 14.9 meV.

Figure 1(a) shows the inelastic neutron scattering spectra for O2-adsorbed Cu2(4-F-bza)4(2-mpyz) at 4.6 K. We observed non-dispersive excitation at 0.4 meV, which cannot be observed in the spectra for the sample after O2 gas evacuation shown in Fig. 1(b). It indicates that the excitation is the magnetic excitation for the adsorbed O2 molecules. In order to obtain the spectra of the adsorbed O2 molecules, we regards the spectra for the O2-removed sample as the background and subtract it from the spectra for O2-adosrbed sample. Figure 2 shows the temperature dependence of one-dimensional Q cuts of the spectra of the adsorbed O2 molecules. The intensity at 0.4 meV decreases with increasing temperature, and is well suppressed at 40 K.

[1] R. Kitaura et al., Science 298, 2358 (2002). [2] T. Masuda et al., J. Phys. Soc. Jpn. 77, 083703 (2008). [3] B. Bussery and P.E.S. Wormer, J. Chem. Phys. 99, 1230 (1993). [4] Y. Takasaki and S. Takamizawa, JACS 136, 6806 (2014).

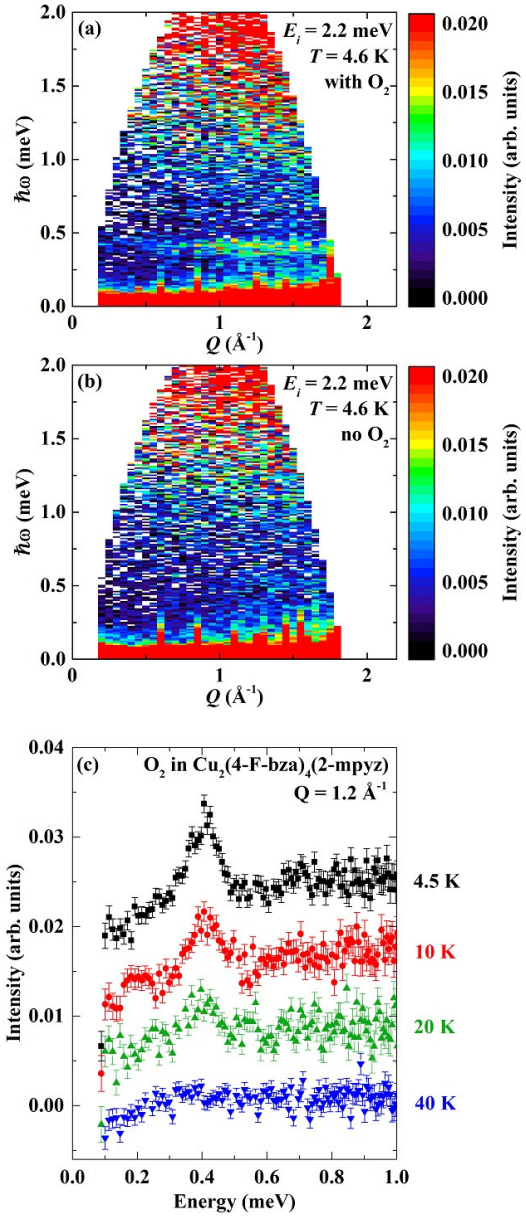

Fig. 1. Inelastic neutron scattering spectra for (a) O2-adsorbed and (b) O2-removed Cu2(4-F-bza)4(2-mpyz) at T = 4.6 K. (c) Temperature dependence of one-dimensional Q cuts for the spectra of the adsorbed O2.

Large magnetic anisotropy induced by high-pressure torsion straining

N. Adachi (A), Y. Oba (B), Y. Todaka (A)
(A) Toyohashi University of Technology, (B) Kyoto University

High-pressure torsion (HPT) is a useful technique to introduce a large amount of lattice defects (dislocations and grain boundaries) in metals and alloys. These changes in crystal structures often bring exotic mechanical and magnetic properties. We have recently found that submicrocrystallined Fe fabricated by the HPT process (HPT-Fe) shows irregular small-angle neutron scattering (SANS) patterns at a high magnetic field. This result exhibits that a spin misalignment in nanometer scale remains even at a magnetic field enough to saturate the magnetization of pure Fe. Therefore, strong magnetic anisotropy is probably induced in Fe by the HPT straining.

To clarify the origin of this strong magnetic anisotropy, the effects of lattice defects and crystal structure were investigated. The amount of lattice defects (dislocation and grain boundary) was controlled by annealing treatment after HPT of Fe. In order to elucidate the relation between the magnetic anisotropy and the crystal structure, the SANS measurement of HPT-Ni was also performed in this study.

The SANS measurements were carried out at the SANS instrument Quokka installed at OPAL, Australian Nuclear Science and Technology Organisation (ANSTO). Four disc samples with the thickness of 0.5 mm were stacked for the SANS measurements. We confirmed that multiple small-angle scattering did not occur from the comparison of the scattering profiles between a disc and four discs. A magnetic field up to 10 T was applied to the samples perpendicular to the incident neutron beam using a superconducting electromagnet.

With decreasing the amount of grain boundaries by annealing treatment of HPT-Fe, the size and volume fraction of the spin misalignment decrease while dislocation density has small effect, suggesting that grain boundaries play important role on the strong magnetic anisotropy in HPT-Fe.

In the scattering profiles of the HPT-Ni, a clear shoulder is observed at the magnetic field of 1 T and becomes small with increasing the magnetic field (Figure). These behaviors are similar to those observed in HPT-Fe. This confirms that the spin misalignment is also generated in HPT-Ni. Therefore, a localized large magnetic anisotropy field is probably induced in a wide variety of magnetic materials by the HPT straining. The scattering intensity observed in HPT-Ni is lower than that in HPT-Fe. This suggests that the lower volume fraction of the spin misalignment and/or lower scattering contrast.

We acknowledge the support of the Australian Centre for Neutron Scattering, ANSTO, in providing the neutron research facilities used in this work. This work was partially supported by JST Collaborative Research Based on Industrial Demand program.

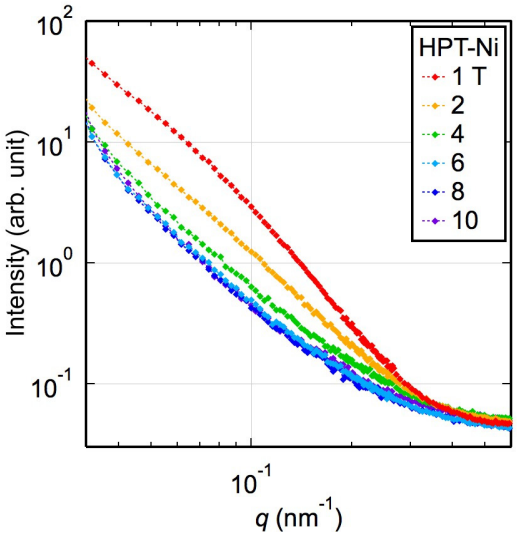

Fig. 1. Scattering profiles of HPT-Ni measured in the magnetic field between 1 and 10 T.

Investigation on magnetic devil's staircase in $La_5Mo_4O_{16}$

Kazuki Iida, Ryoichi Kajimoto, Masaaki Matsuda, and Feng Ye
CROSS, J-PARC Center, and ORNL

Study of competing or frustrated interactions in materials is one of the important issues of the material science, because they often induce interesting magnetic properties. Such competing and/or frustrated interactions sometimes induce a long-period ordered structure whose periodicity shows discrete changes as a function of external field (so-called devil's staircase). This long-period structure is intimately related with the novel phenomena characterizing the materials as seen in recent examples of the stripe ordering in layered Ni perovskite oxides, charge ordering in the spin-ladder compound NaV_2O_5, the multiferroics in $RMnO_3$, and the giant magnetoresistance in $SrCo_6O_{11}$. Recently, we found another material, $La_5Mo_4O_{16}$ that shows the magnetic devil's staircase as a function of external magnetic field (B). In this material, several magnetization steps (e.g. 1/7 plateau) were observed in the magnetization curve under $B \,||\, c$ at 50 K.

$La_5Mo_4O_{16}$ is a layered perovskite compound with monoclinic symmetry, and there are three inequivalent Mo sites (Mo1, Mo2, and Mo3) as shown in Fig. 1(a). Corner-sharing MoO_6 octahedra consisting of Mo1 and Mo2 form a quasi-square checkerboard lattice. Meanwhile, two Mo3 form a Mo_2O_{10} pillar, which is located between the perovskite layers and connects Mo2 octahedra. The valences of the Mo1, Mo2, and Mo3 sites are 5+, 4+, and 4+, respectively, and the Mo1 and Mo2 sites have spins $S = 1/2$ ($4d^1$) and $S = 1$ ($4d^2$). On the other hand, the molecular orbital in the edge-sharing bioctahedral Mo_2O_{10} is in the low spin state. Since Mo_2O_{10} pillars are nonmagnetic and the distance between the layers is large, the interlayer interaction is expected to be very weak. Under zero magnetic field, $La_5Mo_4O_{16}$ undergoes the magnetic phase transition below $T_N = 190$ K, where the in-plane collinear ferrimagnetic structure stacks antiferromagnetically along the c axis [K. Iida *et al.*, J. Phys. Soc. Jpn. **86**, 064803 (2017).]. The antiferromagnetic (AFM) interlayer coupling is fragile against the magnetic field, and $La_5Mo_4O_{16}$ undergoes a ferrimagnetic state with ferromagnetic (FM) interlayer coupling above $B \sim 0.5$ T. Therefore, the devil's staircase phenomenon in the magnetization curve of $La_5Mo_4O_{16}$ can be interpreted as a mixture of the FM and AMF coupled layers and discrete changes of their ratio. However, the actual way of stacking of the layers has not been confirmed due to lack of microscopic measurements. To clarify the period of the long-period ordering gives the fundamental information to understand the devil's staircase phenomenon and important hint of the characters of the competing interactions underlying the phenomenon.

We performed neutron diffraction measurements using a single crystal of $La_5Mo_4O_{16}$ with mass of $\sim$ 40 mg [Fig. 1(b)] under the external magnetic field ($B \,||\, c$) at the single crystal diffractometer CORELLI in SNS to determine the wave vectors characterizing the magnetization steps. We also measured external magnetic field dependences of diffraction patterns in $La_5Mo_4O_{16}$.

Figures 1(c) and 1(d) show the external magnetic field dependences of diffraction patterns of $\left(-1-1-\frac{1}{2}\right)$ (AF) and $(-1-1-1)$ (FM) with field ramping up to 2 T at 50 K. When the field is increased, the AF magnetic peak disappears above 1.2 T [Fig. 1(c)], while the intensity of the FM peak increased above 1.2 T [Fig. 1(d)]. Interestingly, with field ramping down to 0 T, as shown in Figs. 1(e) and 1(f), field dependences of both $\left(-1-1-\frac{1}{2}\right)$ and

$(-1-1-1)$ were different from those of field ramping up. On the other hand, no incommensurate magnetic peak was observed (not shown). These results indicate that $La_5Mo_4O_{16}$ shows the hysteresis as expected for the ferrimagnetic nature, consistent with the bulk magnetic measurements. On the other hand, the 1/7 plateau cannot be explained by the long-priod magnetic structure with the magnetic propagation vetor of $\left(0, 0, \frac{1}{7}\right)$. Instead, the magnetization steps originate in the balance of AF and ferrimagnetic structures (or the domain effect due to the monoclinic structue), which could be explained by a function of temperature and external magnetic field.

The complete data set of neutron diffractions obtained by CORELLI under the external magnetic field will provide us great insights to construct the microscopic model to unserstand the exotic magnetisms in $La_5Mo_4O_{16}$.

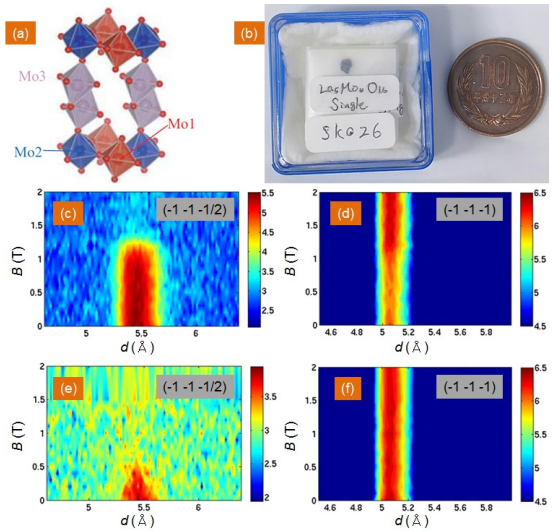

Fig. 1. (a) Crystal structure of $La_5Mo_4O_{16}$. (b) Picture of single crystalline $La_5Mo_4O_{16}$. (c) – (f) External magnetic field dependences of Bragg peaks. (c) and (d) are field ramping up while (e) and (f) are field ramping down.

Low-energy magnetic excitations in YIG

Y. Nambu[1], Y. Okino[1], S. Yano[2], and J.S. Gardner[2]
[1]*IMR, Tohoku University*, [2]*ANSTO*

The spin Seebeck effect (SSE) [1] attracts much attention due to possible application to thermal spin generators for driving spintronics devices. The recent discovery of the SSE in magnetic insulators [2] adds essential information for understanding the physics of the SSE. Originally the SSE was phenomenologically formulated in terms of thermal excitation of conduction electrons, in analogy with the conventional Seebeck effect requiring the existence of itinerant charge carriers. The observed SSE in insulators indicates that there are no needed conduction electrons, but it may be directly associated with magnetic properties in ferromagnetic materials. Uchida *et al*. [3] have recently examined temperature dependence of longitudinal SSE at high temperatures in $Pt/Y_3Fe_5O_{12}$ (YIG) systems. They found that the magnitude of the SSE voltage rapidly decreases with increasing temperature and disappears above the Curie temperature of YIG ($T_c \sim 560$ K), implying the necessity of the ferromagnetism for the SSE. But the critical exponent of the SSE voltage in Pt/YIG was estimated to be much greater than that of the magnetization curve of YIG. This discrepancy indicates that the mechanism of the SSE cannot be explained in terms of simple static magnetic properties and rather calls for a dynamical magnetic interpretation of the effect.

Although YIG is the well-known ferrimagnet and a key material for the SSE, research on dynamical magnetism is limited. To our best knowledge, the only detailed neutron scattering experiment on YIG is investigated on a part of spin excitations by a triple-axis spectrometer [4]. We found several magnetic excitations missed in the previous triple-axis measurement. We therefore used lower energy incident neutron with adequate energy resolution to fully determine coupling constants between irons and to decide Q or Q^2 dependence of the acoustic magnon branches.

Inelastic neutron scattering experiment was carried out on the cold neutron triple-axis spectrometer SIKA at ANSTO, Australia. A single crystal (mass: 8 g) grown by an image furnace is oriented so that the [HHL] plane lies within the horizontal scattering plane. We used a cryofurnace to allow the temperature dependence to be studied between 10 and 450 K. The final energy was chosen either 3.5 or 5.0 meV for access to the relevant wave vector transfer and adequate resolution in the $-1 < \hbar\omega <$ 10 meV energy range. Magnetic excitations from (220) for [110], [001], and [111] directions were nicely observed at 10, 300 K and 450 K. Figure 1 shows magnon dispersion relation along the P[111] direction taken at 300 K. The obtained spectra is compared with spin wave calculation, and preparation for a manuscript is now under way.

[1] K. Uchida et al., Nature 455, 778 (2008). [2] K. Uchida et al., Nat. Mat. 9, 894 (2010). [3] K. Uchida et al., Phys. Rev. X 4, 041023 (2014). [4] J.S. Plant, J. Phys. C 10, 4805 (1977).

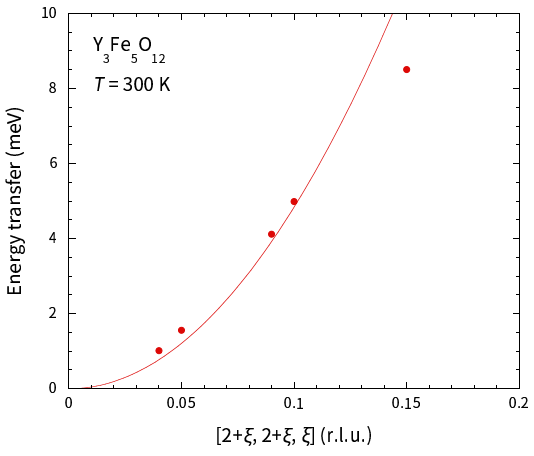

Fig. 1. Magnon dispersion relation along the P[111] direction taken at 300 K.

Polarized neutron scattering investigation of the spin wave excitations in YIG

Y. Nambu[1], Y. Okino[1], T. Kikkawa[1], K. Kakurai[2], B. Winn[3], and J. Tranquada[4]
[1]*IMR, Tohoku University,* [2]*CROSS,* [3]*ORNL,* [4]*BNL*

The observation of the spin Seebeck effect (SSE) by Uchida *et al.* [1] is attracting much attention because this effect can be directly applied to the construction of thermal spin generators for driving spintronics devices, thereby opening the door to thermo-spintronics. The recent discovery of the SSE in magnetic insulators [2] adds an essential piece of information for understanding the physics of the SSE.

Although a systematic investigation of the SSE both in ferromagnetic metals and ferrimagnetic insulators has been performed by means of inverse spin Hall effect (ISHE) measurements [3], no microscopic evidence has been found so far. Recently we performed an inelastic neutron scattering investigation of YIG using the HYSPEC TOF spectrometer. As shown in Fig.1, both magnetic and structural excitations at different zones can be clearly observed. Especially the temperature dependence of the magnetic optical branch at Γ point ($Q = (4, 4, -4)$) compares very nicely with the theoretical spin wave calculation. Since there are low-energy phonon modes clearly visible in these data, an unambiguous investigation of the interesting high temperature behavior of the spin excitations close to T_c and comparison with the theory calls for the utilization of the polarized neutrons. The unambiguous separation of the magnetic and structural excitations and chiral terms as well may also clarify the role of the magnon-phonon coupling in the SSE related compound.

Inelastic polarized neutron scattering experiment was carried out on the chopper spectrometer HYSPEC at SNS, ORNL. Single crystals (mass: 22 g) grown by an image furnace is oriented so that the [HHL] plane lies within the horizontal scattering plane. We used a cryofurnace to allow the temperature dependence to be studied between 35 and 350 K. The incident energy of neutrons was set to 35 meV to cover magnetic excitations from (-4, -4, 4). To achieve σ_x polarization configurations, we put permanent magnets with a yoke to apply magnetic field almost along the wave vector direction. Magnetic excitations are nicely observed, and subtracted chiral terms are also visible by utilizing half-polarized mode.

[1] K. Uchida *et al.*, Nature **455**, 778 (2008). [2] K. Uchida *et al.*, Nat. Mat. **9**, 894 (2010). [3] K. Uchida *et al.*, J. Appl. Phys. **111**, 103903 (2012).

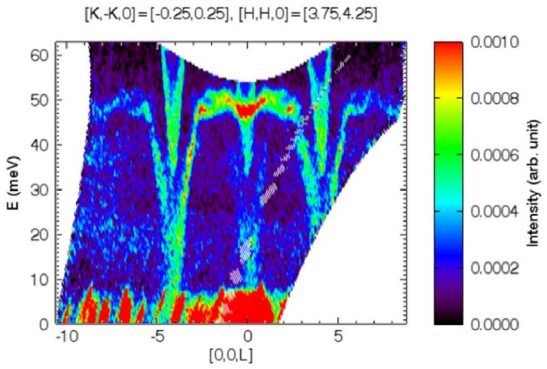

Fig. 1. Magnetic excitations in YIG taken at T = 35 K.

Antiferromagnetic state of Heusler alloy Ru_2CrSi

I. Shigeta[A], M. Hagihala[B], K. Fuchizaki[C], M. Hiroi[A], Y. Nambu[D]
[A]*Kagoshima University,* [B]*University of Tokyo,* [C]*Ehime University,* [D]*Tohoku University*

The first-principles band calculations predicted that $Ru_{2-x}Fe_xCrSi$ is a new type of half-metallic Heusler alloy that is insensitive to crystalline disorder [1]. This insensitivity is worth noting because the spin polarization of well-known half-metallic Heusler alloys, such as Co_2MnSi, is sensitive to crystalline disorder. Our success of synthesizing polycrystalline $Ru_{2-x}Fe_xCrSi$ samples by arc-melting has led us to investigation of their physical properties [2]. With regards to Ru_2CrSi, a clear peak was observed at $\sim$ 14 K in the specific heat $C_p(T)$, indicating the antiferromagnetic (AFM) transition. Partial element substitution of Ru by Fe in Ru_2CrSi seems to suddenly eliminate the AFM order. For $Ru_{1.9}Fe_{0.1}CrSi$, for example, no anomaly in $C_p(T)$ was observed at any temperatures. As far as based on the specific heat measurement, we may conclude that an AFM transition occurs at $T_N \sim 14$ K in Ru_2CrSi.

In this study, we performed the powder neutron diffraction experiments to determine the AFM structure as well as the chemical ordering of the crystal structure at low temperatures in Ru_2CrSi. The experiments have been performed using a powder diffractometer, WAND, installed in HB-2C at the HFIR in the ORNL. A powdered sample (about 11 grams) was loaded in the vanadium cell with the diameter of 9 mm, and then attached to a top-loading liquid helium cryostat. The powder diffraction patterns were recorded in the range from 1.5 K to 290 K.

Figure 1(a) shows the resulting powder diffraction patterns at the low temperatures 1.5 K (red line) and 50 K (blue line). No significant changes in the diffraction patterns were observed on cooling to 50 K, but new peaks appeared below $T_N \sim 14$ K, as shown in Fig. 1(a). Figure 1(b) shows the difference between the patterns observed at 1.5 K and at 50 K, exhibiting that the AFM peaks appeared at low temperature below T_N. Based on the results of Figs. 1(a) and 1(b), we expected that the structure had fcc type-2 AFM order; the magnetic moments were ferromagnetically aligned within 111 planes with adjacent planes coupled antiferromagnetically. However, if the fcc type-2 order was assumed in the AFM structure, we found that the positions of the AFM Bragg peaks in Fig. 1(b) were slightly shifted to low angle, as compare with the positions of the nuclear Bragg peaks in Fig. 1(a). Magnetic as well as crystallographic structure analysis is now in progress using the Rietveld analysis. At the same time, Ru_2CrSi sample quality is also improved by the post-annealing treatment to promote homogeneity and chemical ordering.

[1] S. Mizutani, *et al.*, Mater. Trans. **47** (2006) 25.
[2] K. Matsuda, *et al.*, J. Phys. Condens. Matter **17** (2005) 588; **18** (2006) 1837(E).

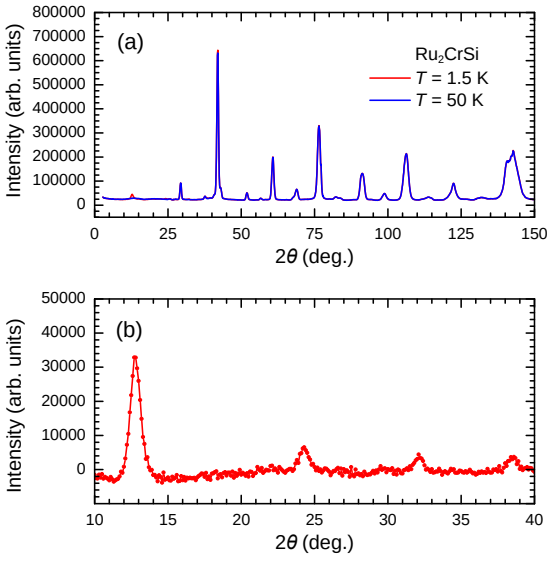

Fig. 1. (a) Neutron powder diffraction patterns at 1.5 K (red line) and at 50 K (blue line). (b) Difference between the patterns at 1.5 K and at 50 K showing appearance of AFM peaks at low temperature.

Uniaxial pressure effect on magnetic ordering in a frustrated isosceles triangular lattice Ising antiferromagnet CoNb2O6

Setsuo Mitsuda, Ryuta Henmi, Takahiro Shimizu
Tokyo University of Science

The isosceles triangular lattice Ising antiferromagnet is characterized by the ratio of exchange interactions defined as $\gamma = J_1$ (along the base direction) $/ J_2$ (along the equilateral direction), and its magnetic property dramatically changes, depending on whether γ is larger than 1.0 or not. As one of the model materials, we have studied an Ising magnet $CoNb_2O_6$, where the quasi-1D ferromagnetic zigzag chains along the c axis form a frustrated antiferromagnetic isosceles-triangular lattice (ITL) with $\gamma \simeq 1.33$ in the a-b plane. If the exchange ratio γ can be controlled in $CoNb_2O_6$ via anisotropic deformation of ITL by uniaxial pressure, variety of interesting magnetic features intrinsic to γ would be observed. Actually along this context, we have succeed in controlling the exchange ratio γ from 1.33 to 1.13 by applying uniaxial pressure p up to 400 MPa along the b axis (J_1 direction), as in the previous experimental reports 21 (N0 1683).

In present experiment, to cross the Wannier point ($\gamma = 1$) and access the region of $\gamma < 1$ by further applying uniaxial pressure p up to 1GPa along the c axis, we performed the neutron-diffraction measurements at the two-axis diffractometer E4 installed at the Berlin Neutron Scattering Center in the Helmholtz Centre Berlin for Materials and Energy. Note that we applied uniaxial pressure along the c axis instead of the b axis, because it turned out in preliminary experiments up to 400 MPa that uniaxial pressure along the c axis have the same effect as one along the b axis.

As shown in the fig.1(a), the exchange ratio γ, which are obtained from the propagation wave number q of sinusoidally-amplitude-modulated incommensurate (IC) state at the phase transition temperature T_1 (from IC to paramagnetic state), shows monotonic decreasing with increasing the applied pressure and crosses 1.0 (Wannier point) at around $p \simeq 700$ MPa. Correspondingly, it can be clearly seen that as the magnetic ground state AF-II magnetic ordering with q=1/ 2 is switched to AF-I magnetic ordering with q=0 at this critical pressure, as shown in fig.1(b). The AF-I magnetic ordering appearing in the region of $\gamma < 1$ is exactly one suggested by Stephenson's exact calculation for 2D ITL. We cursorily investigated $H_{//c} - T$ magnetic phase diagram at p=1 GPa, which should be entirely different from the well-studied phase diagram with AF-II magnetic ordering as a ground state at p=0 Pa. To investigate entire 1 GPa-magnetic phase diagram having newly appearing magnetic state with 1/5 magnetic propagation wave number, further beam-experiment is indispensable.

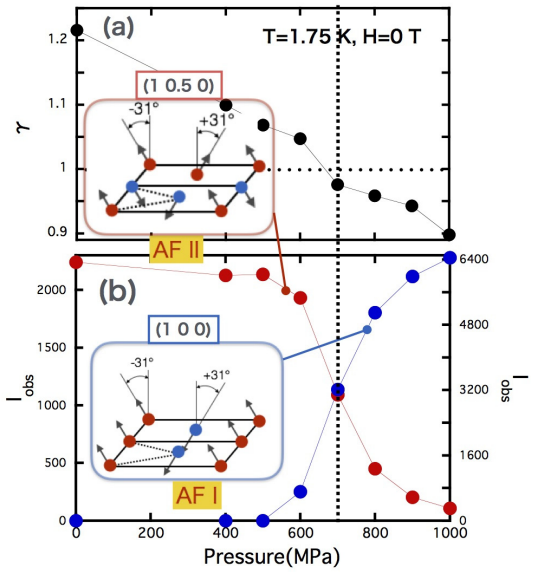

Fig. 1. Uniaxial-pressure p dependence of (a) the exchange ratio γ and (b) integrated intensities of (1 0.5 0) and (1 0 0) magnetic reflections.

Determination of the magnetic structure of the spin-1/2 tetramer compound CuInVO5

Hase M.1, Ebukuro Y.2, Kuroe H.2, and Hester J.3
1NIMS, 2Sophia Univ., and 3ANSTO

Two types of magnetic excitations exist in a magnetically ordered state. They are transverse-mode (T-mode) and longitudinal-mode (L-mode) excitations corresponding to fluctuations in directions perpendicular and parallel to ordered moments, respectively. The T-mode excitations are well known as spin wave excitations, whereas there are a few experimental observations on the L-mode excitations because of their weak intensity. According to the results of theoretical investigations, the L-mode excitations may be observed in an antiferromagnetically ordered state appearing on cooling in interacting antiferromagnetic (AF) spin-cluster compounds [1]. The shrinkage of ordered magnetic moments by quantum fluctuation is important for the appearance of the L mode. If the ground state (GS) of the isolated spin cluster is a spin-singlet state, the shrinkage of ordered moments can be expected in an ordered state generated by the introduction of intercluster interactions.

We focus on spin-1/2 tetramers [2]. The Hamiltonian of the spin tetramer is expressed as H = J1S2S3+J2(S1S2+S3S4). When J1 $>$ 0 and J2 $<$ 0, the GS is a spin-singlet state and an energy difference between GS and first-excited states (spin gap) is much smaller than J1 and |J2|. An ordered state with small ordered moments may be generated by weak intertetramer interactions in spin-1/2 tetramer compounds with J1 $>$ 0 and J2 $<$ 0.

We determined that the spin system of Cu2+ ions in CuInVO5 [3] was interacting spin-1/2 tetramers with J1 = 240 and J2 = -142 K [4]. We confirmed an AF transition at TN = 2.7 K in the specific heat and magnetic susceptibility. We will make single crystals of CuInVO5 and perform Raman scattering measurements to investigate the L-mode magnetic excitations. We will compare experimental results with calculated ones. We need the magnetic structure of CuInVO5 to calculate intensities of one-magnon Raman scattering in the interacting spin-1/2 tetramer model corresponding to CuInVO5.

In the previous measurements on CuInVO5 powder using the Echidna diffractometer (MI5686), we could determine the atomic positions at 5.0 K. However, we could not detect magnetic reflections. We succeeded in the determination of the magnetic structure of CrVMoO7 using the high-intensity powder diffractometer Wombat (P5174) [5]. Therefore, we measured neutron diffraction patterns of CuInVO5 powder using the Wombat diffractometer.

Figure 1 shows diffraction patterns at 1.8 and 5.1 K. The wavelength of neutrons is 0.431 nm. The two patterns overlap almost each other. We madethe difference pattern by subtracting the diffraction pattern at 5.1 K from that at 1.8 K. We could not obtain magnetic reflections, indicating that ordered magnetic moments were small as inferred. The signal to noise ratio is better in the TAIPAN triple-axis spectrometer. We submitted a proposal to determine the magnetic structure of CuInVO5 using the TAIPAN spectrometer (P6336).

Magnetic structure of the magnetic field induced phase in non-centrosymmetric Pr5Ru3Al2

K. Makino(A), D. Okuyama(A), T. Hong(B), T. J. Sato(A)
(A)IMRAM, Tohoku univ., (B)ORNL

Non-centrosymmetric materials are of growing interest recently, because of the possibility for a number of novel phenomena, such as parity-mixed superconductivity in metallic systems, bulk Rashba spin splitting of electron bands in polar materials, and non-trivial spiral or helical spin structures in magnetic materials originating from asymmetric spin-spin interactions. Nonetheless, materials that realize such intriguing phenomena are quite limited, and hence, new non-centrosymmetric materials have been actively sought out recently. Pr5Ru3Al2 is one of such new materials without inversion symmetry [1]. In previous our powder neutron diffraction experiment, we determined the helical magnetic structure with long-period incommensurately modulation vector for Pr5Ru3Al2 below the antiferromagnetic ordering temperature 4.2 K [2]. Interestingly, further phase transition was observed above the 0.1 Tesla magnetic field, suggesting a formation of a complex magnetic phase diagram as shown in Fig. 1 (a). In contrast, there is no details of the microscopic magnetic structure under the magnetic field in Pr5Ru3Al2, but such information is definitely necessary to understand the effect of the loss of inversion symmetry on their magnetic behavior.

To investigate the magnetic structure in Pr5Ru3Al2 under the magnetic field, we performed neutron powder diffraction measurements using C-TAX triple axis spectrometer at HFIR, ORNL. The temperature and magnetic field depdence of the powder diffraction data are shown in Fig. 1 (b - e). At 1.5 K at 0 mangetic field as shown in Fig. 1 (d), we found three incommensurate magnetic reflections, which is consistent with our previous neutron diffraction experiment [2]. At 3.2 K at 0 Tesla, additional two peaks are found. It is clarifed there is additional phase near phase boundary at 0 magnetic field. At 0.15 Tesla magnetic field, the observed diffraction patterns are different with those for 0 magnetic field. At both 1.5 K and 3.2 K as shown in Fig. 1 (b) and (c), the strong intensity is observed near 33.4 degree, which is on the nuclear (1 1 0) position. The magnetic field dependece of the magnetization at 1.5 K shows the magnetic plateau like structure with 1 muB/Pr magnetic moment above 0.08 Tesla, which is 1/3 magnetic moment for the full moment of Pr3+ ion. Thus, the possible magnetic structure at 1.5 K at 0.15 Tesla is ferromagnetic structure with some magnetic moment of Pr in the unit cell aligned to the direction of the magnetic field. At 3.2 K at 0.15 Tesla, the reflection near the nuclear position and the additional small incommensurate reflections are observed. In this phase, the complex magnetic structure with the ferromagnetic and the incommensurate magnetic components would be stabilized.

In summary, we measured the magnetic reflections for the noncentrosymmetric Pr5Ru3Al2 under the magnetic field. From the observed magnetic reflections, further magnetic structure analysis is in progress.

[1] E. V. Murashova et al., Mater. Res. Bull. 45 993 (2010).
[2] K. Makino et al., J. Phys. Soc. Jpn. 85, 073705 (2016)

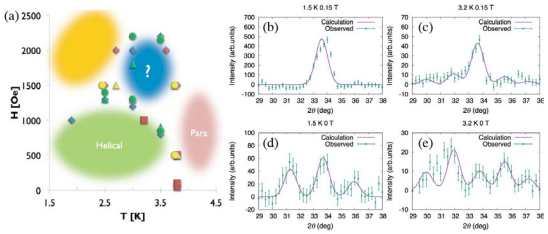

Fig. 1. (a) Phase diagram for Pr5Ru3Al2 determined by the magnetization measurement. Powder neutron diffraction patterns of Pr5Ru3Al2 at 1.5 K and 0.15 Tesla (b), 3.2 K and 0.15 Tesla (c), 1.5 K and 0 Tesla (d), and 3.2 K and 0 Tesla (e).

Strongly Correlated Electron System

Evidence for f-electron multipole ordered phase of PrIr2Zn20

K. Iwasa 1, T. Onimaru 2, K. T. Matsumoto 3, T. Takabatake 2, J.-M. Mignot 4, A. Goukasov 4

Frontier Research Center for Applied Atomic Sciences, Ibaraki University, Japan 1, Graduate School of Science and Engineering, Ehime University, Japan 2, Department of Quantum Matter, Graduate School of Advanced Sciences of Matter, Hiroshima University, Japan 3, Laboratoire Leon Brillouin, CEA-CNRS, CEA/Saclay, France 4

High-rank multipole degrees of freedom of f electrons have been investigated in the context of phase transitions and transport properties owing to coupling with conduction electrons.

One of the typical issues of multipole phenomena is based on a non-Kramers crystalline-field (CF) doublet state with Gamma3 symmetry of f^2 electron configuration under cubic symmetry. This doublet state does not carry magnetic dipole moments, but quadrupoles and octuples. The multipole fluctuation that couples with conduction electrons induce the two-channel Kondo effect (D. L. Cox and M. Jarell, J. Phys., Condens. Matter 8, 9825 (1996)). Such phenomena have been investigated for Pr-based metallic alloy compounds. For example, PrInAg2 shows an extremely enhanced electron mass with the Sommerfeld coefficient of 6.5 J/(mol K 2) without any ordering phase transition down to 50 mK (A. Yatskar et al., PRL 77, 3637 (1996), T. M. Kelley et al., PRB 61, 1831 (2000)).

Recently, several phenomena expected to be relevant to the two-channel Kondo effect are found in a compound series of PrT2Zn20 (T = Ru, Rh, Os and Ir) (T. Onimaru et al., JPSJ 79 (2010) 033704). In particular, PrIr2Zn20, which is investigated in this study, exhibits superconductivity below 0.05 K and a phase transition at 0.11 K (T. Onimaru et al., PRL 94, 197201 (2005)). The latter transition is a signature of the multipole ordering associated with the Gamma3 CF ground state. The evidences of the Gamma3 ground state in PrT2Zn20 were obtained by inelastic neutron scattering from powdered samples using the triple-axis thermal neutron scattering instrument TOPAN installed at JRR-3 and the cold-neutron disk-chopper spectrometer AMATERAS at BL14 of MLF, J-PARC (K. Iwasa et al., J. Phys. Soc. Jpn. 82, 043707 (2013)). In contrast to such localized f-electron behavior, the magnetic entropy at 0.11 K is only 20% of the expected doublet ground state. The most striking features are non-Fermi-liquid (NFL) behaviors in the temperature range just above the ordering point: T^0.5 dependence of electrical resistivity and -lnT dependence of specific heat divided by temperature. These experimental results can be explained by strong interaction between the f electrons and the conduction electrons. The ordered structure is a key issue to understand the unconventional electronic state.

We carried out neutron diffraction measurements for co-aligned single-crystalline samples of PrIr2Zn20 under magnetic fields up to 5 T applied along the cubic [1 -1 0] and [0 0 1] axes. Sample temperatures were controlled down to 40 mK. These conditions were provided by a dilution insert equipped with a cryomagnet installed on the neuron diffractometer 6T2 at Orphee reactor of Laboratoire Leon Brillouin, France. The measurement with magnetic fields along the [1 -1 0] axis was performed in 2015, and the subsequent measurement under magnetic fields direction along the [0 0 1] axis was attempted this time in 2016, in order to observe anisotropic response of the ordered f-electron state against applied magnetic fields.

The upper panel of Fig.1 shows a rocking-curve scan profiles through the scattering vector Q = (0.5, 0.5, 1.5) measured at 40 mK under the magnetic fields along the [1 -1 0] axis. The data at 5 T shows a distinct peak, in contrast to that suppressed at zero magnetic field. Similar magnetic-field-induced reflections were observed at several reciprocal lattice points characterized by the common reduced wave vector Q = (1/2, 1/2, 1/2). The result indicates a long-period ordering of non-magnetic multipole associated with the non-Kramers doublet Gamma3. We also measured temperature dependence of the induced peak. The transition temperature of 0.12 K was determined under the magnetic field of 5 T, which is consistent with that reported in the specific-heat measurement (T. Onimaru et al., PRL 94, 197201 (2005)) and the ultrasonic studies (I. Ishii et al., J. Phys. Soc. Jpn. 80, 093601 (2011)). On the other hand, measurement results for the same scattering vector, Q = (0.5, -0.5, -1.5), under magnetic fields applied along the [0 0 1] axis did not show any induced superlattice reflection, as shown in the lower panel of Fig. 1. This fact indicates that the ordered state does not have any induced magnetic dipole symmetrically inherent in the ordered multipole under the [0 0 1] magnetic fields, so that no staggered configuration of dipole moments appear in spite of the long-period ordered phase. Considering the symmetry classification of quadrupoles within the f-electron CF ground state, we conclude that the long-range antiferro-type order in PrIr2Zn20 is dominated by a Gamma3-type quadruple. It is a further subject how the ordered multipole plays a role in the characteristic low-temperature properties like the NFL behaviors, which are caused by the two-channel Kondo effect.

We thank J.-L. Meuriot and Ph. Boutrouille for technical support on performing the low-temperature neutron diffraction measurements. The experiments were supported by General User Program for Neutron Scattering Experiments, Institute for Solid State Physics, The University of Tokyo, at JRR-3, Japan Atomic Energy Agency, Tokai, Japan.

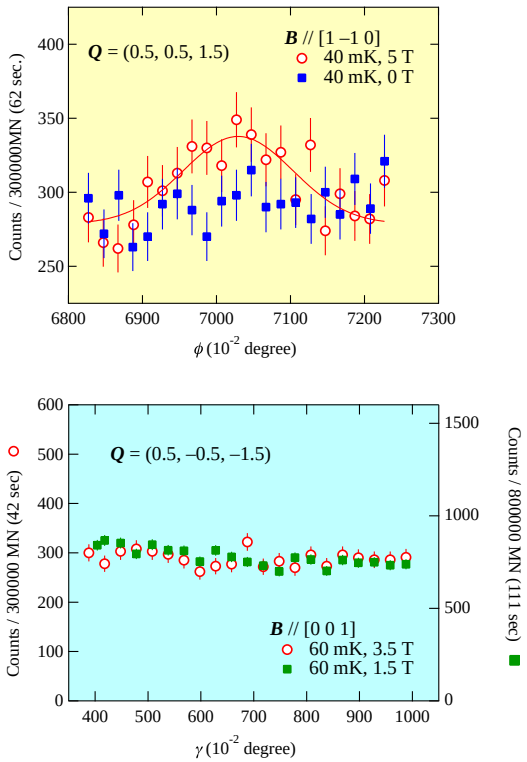

Fig. 1. The scan profiles of the superlattice reflections in the ordered phase at various mgnetic fields.

Uniaxial-pressure control of ferroelectricity in a spin-driven magneto-electric multiferroic CuFeO2

Hiromu Tamatsukuri, Setsuo Mitsuda, Ryuta Henmi
Tokyo University of Science, Department of Physics

A triangular lattice antiferromagnet $CuFeO_2$ exhibits a spin-driven ferroelectric phase (a FE-ICM phase), in which a noncollinear helical magnetic structure breaks inversion symmetry in this system, by substituting a few percent of nonmagnetic Ga^{3+} for magnetic Fe^{3+}. In addition, $CuFeO_2$ is also a strong spin-lattice coupling system, whose magnetic phase transitions are accompanied by crystal lattice distortions owing to the geometrical spin frustration. Therefore, this compound is one of the model materials for investigating novel magneto-electric cross-correlated phenomena induced by anisotropic uniaxial pressure p.

Recently, we found that the application of p along the $[1\bar{1}0]$ direction, which is conjugate to the spontaneous lattice distortion, induces another ferroelectric phase (a FE2 phase) in $CuFe_{1-x}Ga_xO_2$ (CFGO) with x = 0.035. In previous neutron diffraction experiment under applied p of 400 and 600 MPa (NSL-00000329), we revealed that this ferroelectric transition was accompanied by the magnetic phase transition from the OPD phase, as shown in Fig. 1(b). In this study, we have investigated how a phase-boundary line between the OPD and the PD phases starting from the point (p = 0 MPa, T = 13.5 K) meets with a phase-boundary line between the OPD and the FE2 phases in the p-T magnetic phase diagram of the x=0.035 sample, as an extension of previous study.

The neutron-diffraction measurements under applied p were carried out at the two-axis diffractometer E4 installed at the Berlin Neutron Scattering Center in the Helmholtz Zentrum Berlin for Materials and Energy. The wavelength of incident neutron was 2.44 Å. Since the direction of p is parallel to the $[1\bar{1}0]$ direction, the scattering plane is the (HHL) plane.

A magnetic phase transition temperature from the OPD to the PD or the FE2 phases, T_{N2}^{high}, can be determined by temperature dependence of a magnetic wave propagation wave number q; q on cooling starts to vary at T_{N2}^{high} as shown in Fig. 1(a). As a result, we have determined the phase boundary line in the p-T magnetic phase diagram of the x=0.035 sample, as indicated by a red line in Fig. 1(b). We have found that a temperature of ferroelectric polarization emergence, T_{FE2}, corresponds to T_{N2}^{high} above p = 350 MPa, while in a range of 200 MPa $\leq p \leq$ 350 MPa, it does not.

From this experiment, the magnetic structure in the FE2 phase is expected to be the sinusoidal type, which does not break the inversion symmetry in this system as in the PD phase. Since the scattering plane is restricted to the (HHL) plane, however, we can still consider the possibility that there are some tiny modifications from the sinusoidal magnetic structure induced by applied p, and this modified magnetic structure results in the inversion symmetry breaking. To understand the origin of ferroelectricity in the FE2 phase, it is a necessary task to perform more detail magnetic structure analysis in the FE2 phase using magnetic reflections in wider reciprocal lattice space beyond the (H ,H ,L) plane.

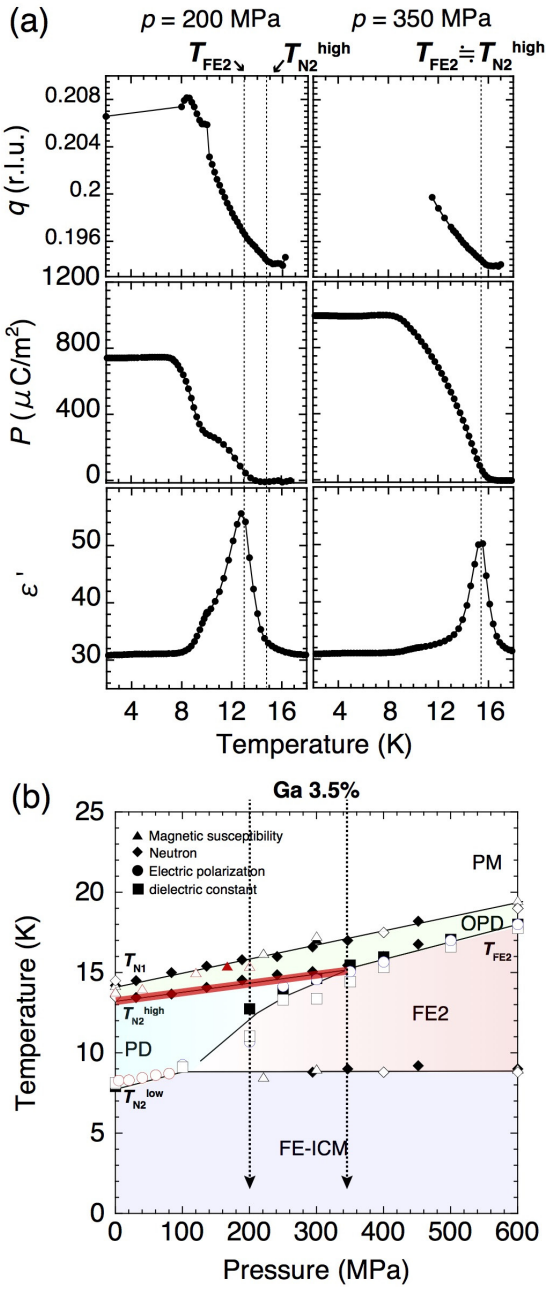

Fig. 1. (a) Temperature dependence of q, P[110] and dielectric constant under p of 200 MPa (left panel) and 350 MPa (right panel). (b) A p-T magnetic phase diagram of a x=0.035 sample. A red line indicates a phase boundary obtained by this experiment.

Small angle neutron scattering on Sr2RuO4

H.Furukawa
Ochanomizu University

Unconventional superconductors have shed light continuously in superconducting field. One of them, Sr2RuO4, is a kind of specials because it has been clamed as a spin triplet (S = 1) superconductor even being isostructural of the high-Tc material La2-xSrxCuO4. In order to study this potential material, we grew single crystals of Sr2RuO4 by floating zone method and tried to observe flux line lattice (FLL) signals by small angle neutron scattering (SANS) technique. The experiment was performed at ultra small angle diffractometer, KWS-3, at Forschungsreaktors Munchen II (FRM II), Germany.

As shown in a figure below, we have succeeded in observing FLL signals at ultra low magnetic fields. (as low as 8mT) A previous work done by Riseman et al.(Nature (London) 396, 242 (1998)) reported that the system shows square FLL at 20mT. The present results indicate that we might be able to follow a FLL structural transition in Sr2RuO4 and we are now submitting a continuous proposal to KWS-3.

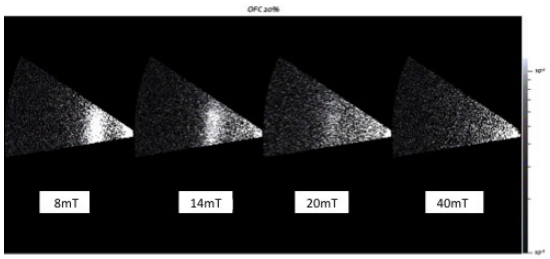

Fig. 1. FLL pattern observed at 8mT,14mT,20mT and 40mT.

Travel expenses to KWS-3 were partially supported by General User Program for Neutron Scattering Experiments, Institute for Solid State Physics, The University of Tokyo (proposal no. 16549), at JRR-3, Japan Atomic Energy Agency, Tokai, Japan. We really appreciate this support since we could not perform this experiment without it.

Vortex study on Fe-based superconductors

H.Furukawa
Ochanomizu University

In order to measure the vortex lattice (VL) in optimal doped Ba0.5K0.5Fe2As2 crystal, we performed a small angle neutron scattering experiment at D33 in ILL. For this experiment, we prepared a new single crystal and set it on an Al plate with [100] and [001] axes horizontal and applied a field along/near the c-axis.

The results revealed that the system shows ring type diffusive diffraction patterns in a low field region but clear spots at higher fields. A figure below shows an example of the diffraction patterns measured with the field slightly rotated away from the c-axis. The six spots pattern indicates that the system has triangle flux line lattice. In this time of experiments, we could measure vortex reflection patterns at several fields but it is limited as being lower than 16 T. The upper critical field for this material is an order of 100T, so we expect to extend this measurement to higher field region. Then now we requested beamtime at EXED, HZB and plan to perform next experiment during summer of FY2017.

Finally, we would like to thank financial support for this travel by ISSP since this experiment could not be done without it.

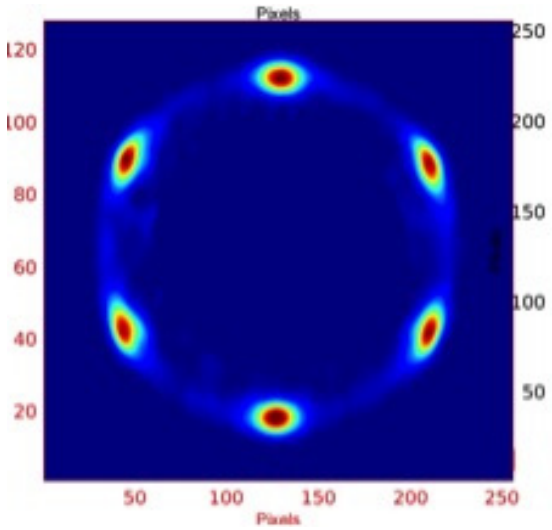

Fig. 1. FLL pattern at 3K with a magnetic field of 16T applying 10deg.off from c-axis.

Weak ferromagnetic superconductor Tb0.47Y0.53Ni2B2C

Misato Takahashi
Ochanomizu Univ.

“ Spontaneous vortex phase ” in a ferromagnetic superconductor is one of the issues that have not been confirmed yet. Previously we studied ErNi2B2C (Tc = 10.5 K), but due to the fact that weak ferromagnetic (WFM) transition temperature of the system (TWFM = 2.3K) is lower than its superconducting transition temperature Tc, confirmation of such an exotic state was not conpleted. In order to duly confirm a spontaneous vortex phase, we next choose TbxY1-xNi2B2C as a system that should have a region with TWFM being higher than Tc [1,2]. From the phase diagram, we choose x = 0.47 as a target Tb concentration and grew single crystals of Tb0.47Y0.53Ni2B2C (Fig.1). Magnetization data indicate that the system posses an AF transition at 6K, a WFM one below 4K and a superconducting one below 2K.

To verify the WFM state and to determine the magnetic structure in antiferromagnetic (AFM) and WFM phases, we proposed neutron elastic measurements and performed such experiments from 11th to 15th Aug. 2016 at cold neutron triple axis spectrometer (CG-4C), HFIR in ORNL.

We first measured neutron diffraction profiles at (h 0 1) at 10 K, (the paramagnetic phase), 3 K, (the AFM phase) and 0.25 K, (the WFM phase) (Fig.1). Below TN in addition to the nuclear peaks observed at 10 K, a clear magnetic Bragg peak appeared at (0.450 0 1). But no magnetic peak was observed at (0.550 0 0), indicating that magnetic moments on Tb atoms form a longitudinal spin density wave (SDW) order with a propagation vector of q = 0.550a*. Fig.2 shows temperature dependence of integrated intensity of the (0.45 0 1) peak. We also measured field dependence of the SDW peak under fields parallel to the [0 1 0], and confirmed that it disappeared above 2 T. 2 T is too small to attribute this to saturation of the Tb moments along the field direction and so it was attributed to an occurrence of a magnetic structure transition. To verify the WFM state, temperature dependences of intensities at nuclear Bragg points (0 0 1) and (1 0 1) were measured. But we could not detect the evidence of the WFM order. So as a next step, we would like to propose polarization analysis for the temperature dependence of (0 0 6) peak, since nuclear intensity at this position is relatively weak.

This travel was done with a financial support by ISSP, University of Tokyo. We appreciate it pretty much since it could not be done without it.

References

[1] B. K Cho et al., PRB. 63 (2001) 144528.
[2] Mater and Bachelor theses at Furukawa Lab. @ Ochanomizu University.

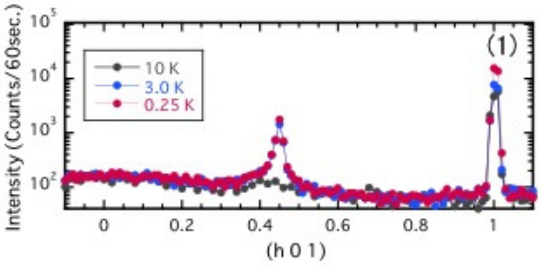

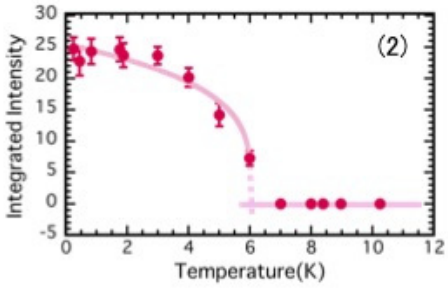

Fig. 1. Temperature dependence of the neutron diffraction profiles at (h 0 1) Fig. 2. Temperature dependence of integrated intensity of (0.45 0 1) peak

Weak ferromagnetic superconductor Tb0.47Y0.53Ni2B2C

Misato Takahashi
Ochanomizu Univ.

" Spontaneous vortex phase " in a ferromagnetic superconductor is one of the issues that have not been confirmed yet. Previously we studied ErNi2B2C (Tc = 10.5 K), but due to the fact that weak ferromagnetic (WFM) transition temperature of the system (TWFM = 2.3K) is lower than its superconducting transition temperature Tc, confirmation of such an exotic state was not completed. In order to duly confirm a spontaneous vortex phase, we next choose TbxY1-xNi2B2C as a system that should have a region with TWFM being higher than Tc [1,2]. From the phase diagram, we choose x = 0.47 as a target Tb concentration and grew single crystals of Tb0.47Y0.53Ni2B2C (Fig.1). Magnetization data indicate that the system posses an AF transition at 6K, a WFM one below 4K and a superconducting one below 2K.

The previous neutron diffraction measurements at C-TAX let us confirm that the system has a longitudinal spin density wave (SDW) order with a propagation vector of q = 0.550a* below 5K, and another magnetic transition between 1 T and 2 T. However we could not confirm the WFM order due to limitation of Q range. Then in the present study, to confirm the WFM order, we proposed polarized neutron measurements and performed experiments from 17th to 20th January, 2017, at thermal neutron polarized triple axis spectrometer (HB-1), HFIR in ORNL. We performed half polarized analysis and measured temperature dependences of integrated intensities at nuclear Bragg points (0 0 2) and (0 0 6). Both zero field cooled and field cooled data under fields of 0.05 T, 0.1 T, 0.5 T and 2 T were measured.

Fig.2 shows temperature dependences of integrated intensities at (006) under 0.1 T along [010]. Here I+ (and I-) indicates scattering intensity with incident neutron spins being parallel (anti-parallel) to the WFM moments (so a guide field). The data show two anomalies at around 6.0 K and 2.5 K. After comprehensive analysis, we interpreted that the change at around 6.0 K could be attributed to the crystal structural (tetragonal?orthorhombic) phase transition accompanied by the SDW one and that at 2.5 K to the ferromagnetic one.

This travel was done with a financial support by ISSP, University of Tokyo. We appreciate it pretty much since it could not be done without it.

References

[1] B. K Cho et al., PRB. 63 (2001) 144528.
[2] Mater and Bachelor theses at Furukawa Lab. @ Ochanomizu University.

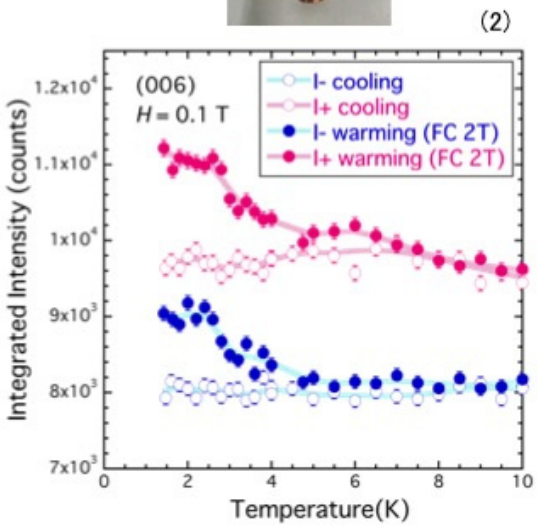

Fig. 1. Single crystals of Tb0.47Y0.53Ni211B2C Fig. 2. Temperature dependences of integrated intensities at (006) Bragg point

Determination of the Magnetic Structure of the Noncentrosymmetric Heavy-Electron Metamagnet $CePdSi_3$

M. Yoshida, D. Ueta, T. Kobuke, H. Yoshizawa
The Institute for Solid State Physics, The University of Tokyo

The influence of antisymmetric spin-orbital interaction (ASOI) caused by the lack of inversion symmetry has attracted much attention since the discovery of the first heavy electron superconductor $CePt_3Si$. Recently, we have reported that the non-centrosymmetric $BaNiSn_3$-type compound $CePdSi_3$ exhibits successive magnetic transitions, weak ferromagnetism (canted antiferromagnetism) and metamagnetic transitions, yielding an unusually complex $H-T$ phase diagram (D. Ueta et al., J. Phys. Soc. Jpn., 85, 104703 (2016).). Although $CePdSi_3$ is one of the most promising candidates to clarify the influence of ASOI upon physical properties due to a possibility that this complex $H-T$ phase diagram may result from the ASOI effect, magnetic structures in all phases has not been undetermined yet.

In order to determine magnetic structures at zero field in $CePdSi_3$, we performed elastic neutron scattering experiments at BL-09 (CORELLI), SNS in Oak Ridge National Laboratory. A single crystalline sample of $CePdSi_3$ was grown by flux method in the Institute for Solid State Physics. The sample was mounted on an Al pin such that both a and c axes are set into the equator plane and installed in the orange cryostat. Temperature range was from $\sim$ 1.45 K to 10 K.

Figure(a) shows a part of the (H, -1, L) contour map around (0, -1, 1) reflection at based temperature. We have observed clear magnetic satellite peaks around nuclear Bragg reflections and found the magnetic propagation vector at base temperature is $q \sim$ (0.3, 0, 0). Subsequently, we measured temperature dependence of several nuclear reflections and satellite peaks. As one example, we show the temperature dependence of integrated intensity of sum of the magnetic satellite peaks Q = ($\pm$0.3, -1, 1) in Figure(b). The slope changes two phase boundary between the phase I and II determined by our preceding study.

Travel expenses were supported by General User Program for Neutron Scattering Experiments, Institute for Solid State Physics, The University of Tokyo (proposal no. 17507), at JRR-3, Japan Atomic Energy Agency, Tokai, Japan.

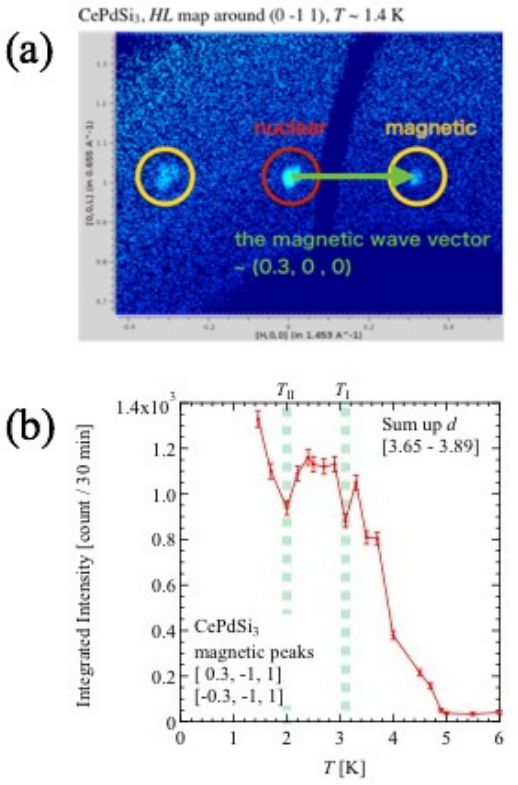

Fig. 1. (a) A part of the (H, -1, L) contour map around (0, -1, 1) reflection at based temperature. (b) The temperature dependence of integrated intensity of sum of the magnetic peaks Q = ($\pm$0.3, -1, 1).

Neutron spin echo measurements on the iron-based ladder compound BaFe2Se3

Y. Nambu[1], M. Nagao[2]
[1]*IMR, Tohoku University,* [2]*NCNR, NIST*

Since its discovery, research on iron-based superconductivity (SC) has become the main stream in condensed matter physics. To gain further insight into the mechanism of SC and variation of magnetism, investigation of Fe-based compounds over distinct spatial dimensions is important. This is because the dimensionality strongly influences magnetism and can control itinerancy of electrons by changing Fermi surface topology.

We have examined magnetism of Fe-based ladder compounds AFe_2X_3 (A = Rb, Cs, Ba; X = S, Se) [1,2], and found the first SC [3]. This is known as the one-dimensional analogue of the Fe-based superconductors. As for parent compounds of the Fe-based superconductors, this family shows 3D magnetic ordering. However, anomaly at the magnetic transition is not visible by bulk properties. Only neutron diffraction can determine transition temperature. Here we concentrate on $BaFe_2Se_3$. We have determined block-type magnetic structure below $T_N = 255$ K through powder neutron diffraction [1]. Magnetic moments (2.8 μ_B at 5 K) are arranged to form an Fe_4 ferromagnetic unit perpendicular to the ladder direction, and each Fe_4 block stacks antiferromagnetically. However, Moessbauer experiment by our collaborators concludes that there is no anomaly at T_N, and hyperfine splitting due to the magnetic transition appears 230 − 240 K. Even below those temperatures, there is a gradual formation of magnetic ordering, and it finally falls into the ordered state $\sim$ 10 K, being consistent with hindered entropy release evidenced by the specific heat data. This distinct behavior could be originating from the difference in timescale of the experimental technique; neutron has 10^{-13} to 10^{-12} sec timescale, being faster than Moessbauer (10^{-7} sec). It should be possible to trace temperature evolution of spin dynamics with the neutron spin echo technique.

Neutron spin echo experiment was carried out on NGA NSE at NCNR, NIST. The wavelength of neutrons was set to 6 and 5 A, and data were taken at $Q = 0.73$ A^{-1} for $5 < T < 250$ K. Echo-mode measurements were performed between Fourier time 0.008 and 17.45 nsec with utilizing " shorty " mode. Relaxation behavior in intermediate scattering function is not so visible, only gradual elevation appears. Figure 1 summarizes averaged intermediate scattering function as a function of temperature. Volume fraction of spins fluctuating faster than measured Fourier time scale changes over wide temperature regime. Combining with other neutron and muon data, quantitative understanding of dynamic magnetism of $BaFe_2Se_3$ is now under way.

[1] Y. Nambu *et al.*, Phys. Rev. B **85**, 064413 (2012). [2] F. Du *et al.*, Phys. Rev. B **85**, 214436 (2012). [3] H. Takahashi *et al.*, Nat. Mat. **14**, 1008 (2015).

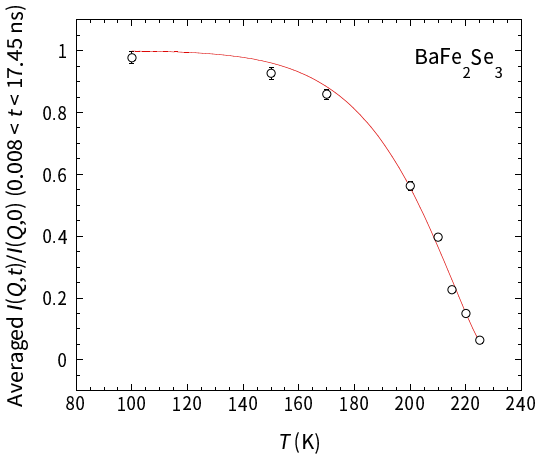

Fig. 1. Averaged intermediate scattering function of BaFe2Se3 as a function of temperature

Domain Formation and Ground State of Spin and Charge Order for RFe2O4 (R=Yb and Lu)

Kosuke Fujiwara1, Yohei Okuda1, Tomoyuki Karasudani1, Naoshi Ikeda1, Kazuhisa Kakurai2

1, Grad. Sch. Nat. Sci. and Tech, Okayama univ. 2, Comprehensive Res. Org. for Sci. and Soc.

The compound family RFe2O4 (R=Dy - Lu, and Y) has attracted much attention due to the possible multiferroic behavior arising from charge ordering. The crystals of these materials belong to the rhombohedral system. The Fe ions are arranged to form the hexagonal double layers and stack in the sequence of (AB), (CA), (BC),... along the rhombohedral unique axis. The average valence of the Fe ions is expected to be Fe+2.5 in these materials and hence a mixed valence state of Fe2+ and Fe3+ ions occupying the equivalent Fe sites on the hexagonal plane with equal probability is expected. Especially LuFe2O4 attracted a lot of attention, because experimental evidence was reported for a ferroelectricity arising from electron correlations in this frustrated triangular mixed valence oxide[1]. It also shows very complex charge and magnetic correlations with finite correlation lengths in zero and applied magnetic field[2]. Despite the intensive investigations on charge and magnetic ordering using both synchrotron x-ray and neutrons, the understanding of the physics in LuFe2O4 is far from complete.

Recently, we succeeded in making a fine stoichiometric crystal of YbFe2O4 and LuFe2O4 with the Floating Zone melting method in which the amount of the iron vacancies was controlled[3]. We found that a single crystal having less iron vacancy has longer spin coherence length and do not show the low temperature spin transition, as called TLT transition. This fact indicates that the unsettled discussion about the spin and charge structure on this material may arise from such iron stoichiometry effect of the crystal. We call such a sample having less iron vacancy as the stoichiometric sample.

We made three dimensional reciprocal space observation for YbFe2O4 using the wide-angle neutron diffraction instrument WOMBAT equipped with two dimensional neutron detector installed at OPAL neutron facility in ANSTO, Sydney, Australia. Also the magnetic component of the signal was examined with 3He spin polarizer and analyzer. Through the experiment, we found typical patterns of charge order signal and its modulations. In figure 1, we show three kind of super lattice points and its modulation in reciprocal space. These signals are found on (1/3 1/3 L) where L is integer and half integer, and (0 0 1.5+3n) where n is integer.

We applied the monoclinic charge order super lattice cell and its possible domain formation to interpret the modulated structure of the super lattices. Then all super lattice signals distributed in reciprocal space are successfully explained. This is the first result in explaining the extinction rule of super lattices of RFe2O4.

It was found that the super lattice signals of (1/3 1/3 L) develops below 390K, which indicates the three dimensional charge ordering transition (3DCO) at this temperature, that is slightly higher than the previous report of T3DCO of non-stoichiometric material.

Below 300K, a characteristic magnetic diffuse scattering appears along (1/3 1/3 L), indicating a short range spin correlation long c-axis, as shown in figure 2. Also the signal of (0 0 m) where m is half integer develops below 300K. Non-magnetic origin of (0 0 m) was confirmed with polarizer analysis. This is an indication of some kind of coupling between lattice modulation and short range spin correlation below 300K. So we expect a possible magneto-

lattice coupled phenomenon in this temperature range.

We also made the two-dimensional reciprocal space observation of the stoichiometric LuFe2O4. The experiment was performed using wide-angle neutron diffraction instrument WAND equipped with one dimensional neutron detector installed at HFIR neutron facility in Oakridge National Laboratory, Tennessee, USA.

The (h h l) plane mapping at 125K for the stoichiometric LuFe2O4 crystal of less iron vacancy is shown in figure 3. Although the diffuse magnetic scattering along (1/3 1/3 L) line in this temperature range has been previously reported in iron deficient non-stoichiometric LuFe2O4, our data shows only the super lattice spots on (1/3 1/3 L) without the diffuse component along L. With the observation of the temperature variation of macroscopic magnetization of this sample, we concluded the vanishing of low temperature spin transition TLT in stoichiometric LuFe2O4. The 3D charge ordering temperature was confirmed at 360K, which is also slightly higher than previous report of non-stoichiometric LuFe2O4.

As the WAND data do not have the three dimensional information in reciprocal space, we have not yet obtained the detailed structure of super lattice and its modulation in LuFe2O4. But the observed anisotropic structures of the super lattice spots may be accounted for by the 2-D projection of the diffraction patterns similar to fig. 1.

The essential conclusions were obtained as follows, 1) the stoichiometric RFe2O4 do not show the low temperature spin transition TLT. Previous report of TLT might arise from a vacancy and its pinned effect for the short range spin ordered region. 2) The three dimensional charge ordering transition of stoichiometric RFe2O4 is slightly higher than 360K. 3) Below 300K, we can expect an unknown lattice and spin coupled phenomenon.

References

[1] N. Ikeda, et al., Nature 436 (2005) 1136.
[2] J. de Groot, et al.,?Phys. Rev. Lett., 108?(2012) 037206.
[3] K. Fujiwara, et al., Trans. Mat. Res. Soc. Japan 41[1] (2016) 139-142.

captions

Figure 1 Three kind of super lattice points and its modulation of stoichiometric YbFe2O4 found 3D reciprocal space. Spots are projected on three planes. I-type and X-type modulations are found on (1/3 1/3 L) position, where L is integer or half integer. -type one is found on (0 0 1.5+3n) position, where n is integer.

Figure 2 Magnetic diffuse scattering along (1/3 1/3 L) of stoichiometric YbFe2O4 appears below 300K.

Figure 3 The (h h l) plane mapping at 125K of stoichiometric LuFe2O4 crystal. No diffuse scattering was found along (1/3 1/3 L) line, indicating no conflicting interaction between ferro- and anti-ferro ordering of spins.

Fig. 1

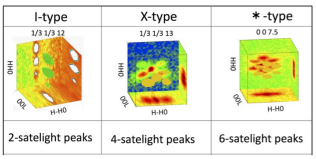

Fig. 2

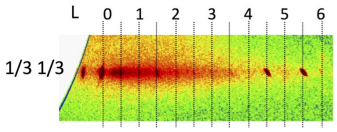

Fig. 3

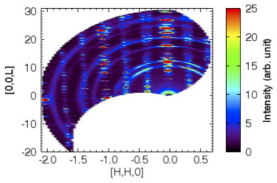

Fig. 1. Captions are given in text.

Biology

Subunit exchange study on alpha-crystallin hetero-oligomer

Rintaro Inoue, Masaaki Sugiyama, Nobuhiro Sato, Yojiro Oba
Research Reactor Institute, Kyoto University

α-crystllinexists as oligomers consisting of a total of about 20~40 subunits of two homologues: α A and α B. The most fascinating and interesting feature of α-crystllin is its chaperone activity, suppressing the onset of abnormal aggregation of various target proteins. However, the detailed mechanism of chaperone activity in α-crystllin is still a matter of discussion. α-crystallin does not possess fixed quaternary structure rather“ dynamic quaternary structure ” induced by reorganization of constituting subunits in α-crystllin. One of the candidates for elementary step for dynamic quaternary structure must be subunit exchange between α-crystllin oligomers. We applied deuteration-assisted small angle neutron scattering (DA-SANS) method on recombinant α-crystllin. Especially, we have prepared partially deuterated (75% deuterated) α-crystllin. From preliminary calculation, it was estimated that 75% deuterated is nearly contrast matched in 100% D2O. We focused on subunit exchange between hydrogenated α A-crystallin and 75% deuterated α B-crystallin under the mixing ratio of 3:1, mimicking the native eye lens environment. DA-SANS experiment was performed with Quokka at 37 C at the time interval of 15 min. Fig. 1 (A) shows the scattering profile from 75% deuterated α B-crystallin in 0%, 60% and 100% D2O buffer. It can be clearly seen that 75% deuterated α B-crystallin was matched out in 100% D2O buffer, certificating the proper deuteration level of partially deuterated α B-crystallin. Fig. 1(B) shows the time dependence of forward scattering (I(0)) after mixing 75% deuterated α B-crystallin and hydrogenated α A-crystallin. Decrease of I(0) was observed, implying the existence of subunit exchange between α B-crystallin and hydrogenated α S?crystallin. Interestingly, it was found that about half of the constituting subunits in oligomeric α A-crystallin was exchangeable from the fit to the time dependence of I(0). At present, biological interpretation for the difference of subunit exchange between homo-oligomeric α B-crystallin and hetero-oligomeric is not obtainable. The complementary studies with mass spectrometry and small angle X-ray scattering (SAXS) are on going.

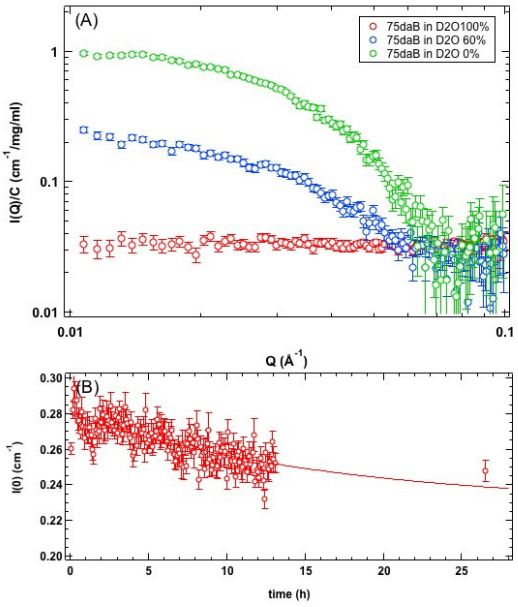

Fig. 1. (A) 75% alpgaB-crystallin in 0%, 60% and 100% D2O buffer. (B) Time evolution of I(0) of 75% deuterated α B-crystallin and α A-crystallin with the mixing ratio of 1:3.

Soft Matters

Structure of imidazolium-based ionic liquid under shear flow

F. Nemoto[1], M. Nagao[2,3], K. Weigandt [2], H. Seto[1],
Y. Kitazawa[4], M. Hirasawa[4], T. Ueki[5], M. Watanabe[4]
[1]*IMSS, High Energy Accelerator Research Organization,*
[2]*NCNR, National Institute of Standards and Technology,* [3]*CEEM, Indiana University,*
[4]*Sch. Eng., Yokohama National University,* [5]*National Institute for Materials Science*

" Ionic liquid " (IL) is a generic chemical name for novel ionic compounds which are in liquid states around room temperature. Alkyl-methylimidazolium-based ILs abbreviated to C*n*mimX, where *n* indicates number of carbons in an alkyl-chain and X is an anion, are most intensively studied in terms of physical properties of ILs. Recent researches using x-ray and neutron scattering in C*n*mimX revealed nanoscale structures, which are characteristic of molecular arrangements between polar- and nonpolar domains [1-3]. Since the molecular length is some 10 Å, characteristic scattering due to the layer structure appears in small scattering angles. ILs are also considered to be useful as lubricants because they remarkably protect moving elements from wear and reduce friction [4]. Indeed, structural rearrangements and change in the rheological behavior have been observed in confined ILs [5]. As it is suggested in surfactant systems, bicontinuous sponge phase with a short-range layer structure is aligned at the solid surface [6], and it is also shown that shear thinning occurs and the layer structure grows under shear flow [7]. Since the lyotropic surfactant bilayers and the domain structure of ILs are somewhat analogous, it is expected that the sliding of such layers in ILs under shear flow help reducing friction. These backgrounds in mind, we performed structural investigations of ILs under shear flow using SANS in order to pursue understanding the relation between the viscoelastic properties and the mechanism of reducing friction.

Since C8mimCl at liquid state shows relatively high viscosity [8] and the time scales for flow and diffusion motions are likely to be comparable at an available shear rate, we expect to see a structural change. A simultaneous small-angle neutron scattering and rheology experiment was performed on NGB-10m SANS at NIST to access high enough Q values with the rheo-SANS set up. Only radial configuration, which corresponds to a plane of normal and lateral direction to the flow, was measured in the present experiment. A scattering peak due to the nanostructure in the IL is measured. The peak was analyzed using a fit to a Lorenzian function.

Fig. 1. shows the shear rate, $\dot{\gamma}$ dependence of the apparent viscosity, η, the peak position, Q_0, and its width, Γ, at 10°C. Shear-thinning behavior, i.e.; η decreases with shear rate $\dot{\gamma}$, is confirmed. At $\dot{\gamma} \leq 200$ s^{-1}, Q_0 and Γ slightly decreased, suggesting the growth of the ordering of the domain structure with increasing the spacing due to the shear alignment effect. However, Q_0 and Γ increased at higher $\dot{\gamma}$, corresponding to the disordering of the structure.

References

[1] A. Triolo *et al.*, J. Phys. Chem. B **111**, 4641 (2007).
[2] M. Kofu *et al.*, J. Phys. Chem. B **117**, 2773 (2013).
[3] F. Nemoto *et al.*, J. Phys. Chem. B **119**, 5028 (2015).
[4] A. E. Somers *et al.*, Lubricants **1**, 3 (2013).
[5] K. Ueno *et al.*, Phys. Chem. Chem. Phys. **12**, 4066 (2010).
[6] W. A. Hamilton *et al.*, J. Chem. Phys. **116**, 8533 (2002).
[7] L. Porcar *et al.*, Langmuir **19**, 10779 (2003).
[8] M. Kofu *et al.*, J. Chem. Phys. **143**, 234502 (2015).

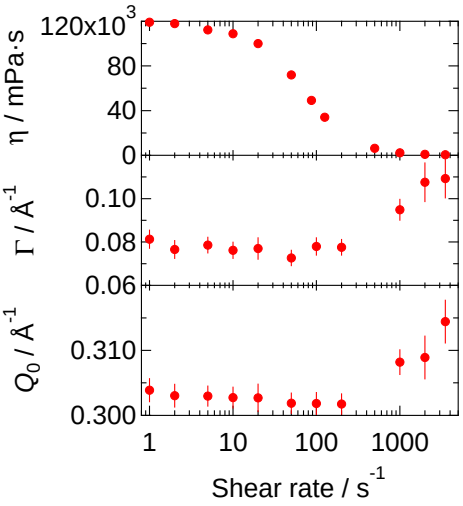

Fig. 1. Shear rate dependence of apparent viscosity η, peak position Q_0 and HWHM of the peak Γ of C8mimCl at 10 °C obtained from the rheo-SANS experiment.

Structural study on the "nonswellable" hydrogel

S. Nakagawa (1), X. Li (1), and M. Shibayama (1)
(1) Institute for Solid State Physics, University of Tokyo

Hydrogels are an important class of soft materials particularly in the medical and bio-science fields. In general, hydrogels swell with water due to the osmotic pressure imbalance inside and outside the gel. Swelling leads to a significant mechanical deterioration and volume expansion, which may cause serious damage to the surrounding tissues when the gel is used in the body.

Recently, we developed a nonswellable thermo-responsive hydrogel synthesized by end-linking between four-armed poly(ethylene glycol) (Tetra-PEG) and four-armed poly(ethyl glycidyl ether-co-methyl glycidyl ether) (Tetra-PEMGE). While PEG is a well-known hydrophilic polymer, PEMGE is a thermo-responsive polymer exhibiting lower-critical solution temperature (LCST) type phase behavior in aqueous solution. When the hydrogel was heated above a certain transition temperature, Tetra-PEMGE units became hydrophobic and started to shrink, resulting in macroscopic shrinking of the entire hydrogel. In the previous study, we found that the equilibrium swelling ratio of the hydrogel was ca. 300% at 10 °C, whereas it decreased dramatically to be ca. 100% at 37 °C, i.e. the physiological temperature. Hence our hydrogel was practically nonswellable in the human body. Interestingly, the hydrogel remained transparent even after shrinking of Tetra-PEMGE units, indicating the formation of a structure with the length scale much smaller than the visible light wavelength. In the present experiment, we carried out small-angle neutron scattering (SANS) measurements on the nonswellable hydrogel to clarify the structural origin of its nonswellable feature.

SANS measurements were performed using QUOKKA at the OPAL reactor in ANSTO, Australia, with the wavelength of 5 A and each of three different sample-to-detector distances of 1.3, 8, and 20 m. The sample temperature T was controlled by the 20-position temperature-variable sample changer. The SANS profiles were corrected for absorption, cell scattering, and solvent scattering. To avoid complications in the model fitting process, the data were further corrected for instrumental smearing by an iterative desmearing algorithm.

Fig. 1 shows the representative SANS profiles of the nonswellable hydrogel at various temperatures. At T lower than 16.6 °C, the profiles are simple; they contain an upturn in the low-q region and a shoulder in the high-q region. The upturn in the low-q region is due to the large-scale aggregation of PEG end-groups and has been observed even in aqueous solutions of PEG. The shoulder in the high-q region reflects the concentration fluctuation of the polymer network and can be explained by the Ornstein-Zernike function, as shown with the solid curves in Fig. 1. However, at T higher than 19.5 °C, an intense peak emerges in the low-q region, which is accompanied by an additional shoulder and small peak in the high-q region at even higher temperatures. The SANS profiles suggest that a nanometer-scale discrete domain structure is formed upon shrinking of Tetra-PEMGE units. The low-q peak and high-q features should reflect the inter-domain correlation (structure factor) and intra-domain correlation (form factor), respectively.

We performed the model fitting analysis on the SANS profiles to extract quantitative information on the domain structure. The spherical domains with the modified hard-sphere interaction were assumed. The model scattering function, shown with the solid curves in Fig. 1, successfully explains

the experimental SANS profiles particularly in the high-q region. We estimated the mean aggregation number N, defined as the number of four-armed prepolymer units contained in one spherical domain, from the structural parameters obtained by model fitting. Strikingly, N was 14 - 21, which was much larger than unity. This clearly indicates that multiple Tetra-PEMGE units as well as Tetra-PEG units aggregate into a single spherical domain. The formation of such relatively large domains causes the significant distortion of the network in the matrix phase, rendering our hydrogel nonswellable.

In summary, we investigated the microscopic structure of the nonswellable hydrogel using SANS and revealed that the formation of spherical domains each containing multiple prepolymer units was responsible for the nonswellable feature. The findings in this experiment will help designing the nonswellable hydrogels and contribute to fundamental understanding of amphiphilic polymer network systems.

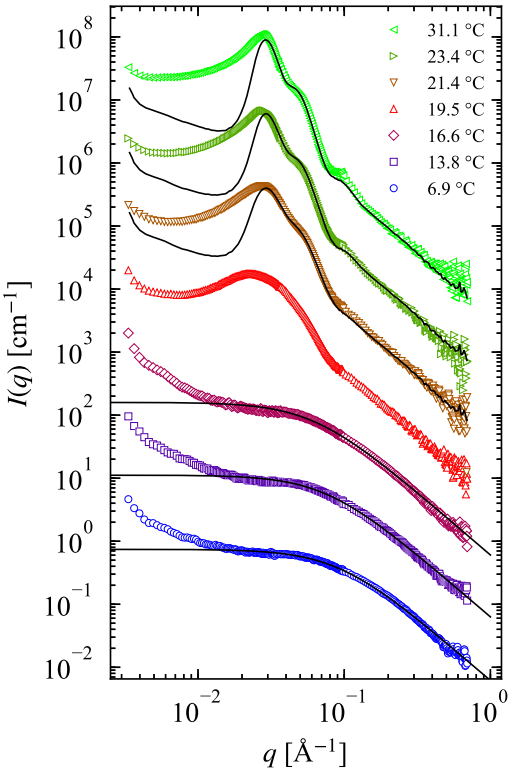

Fig. 1. SANS profiles of the nonswellable hydrogel at various temperatures. Solid curves represent the fitting results.

Structure of Polyelectrolytes under Electric Field

Xiang Li, Mitsuhiro Shibayama
ISSP, University of Tokyo

Polyelectrolytes are polymers whose repeating units bear electrolyte groups. In aqueous solutions, these electrolyte groups dissociate and make the polyelectrolyte charged. Because of the charged groups, the polyelectrolytes are sensitive to salt (size, valence, and concentration), pH, temperature, and electric field. These unique features attract many applications such as superabsorbent material, micro-sensors, and drug-delivery system. Experimental and theoretical studies have been done to investigate the structure of polyelectrolytes in aqueous solutions, using a wide range of techniques including various scattering technics (light, neutron and X-ray) as well as viscoelastic measurement. Through small angle neutron scattering (SANS) and small angel X-ray scattering (SAXS) measurement, a broad peak was observed in the scattering intensity curves of polyelectrolytes solutions when the polymer concentration c was higher than the overlapping concentration c*. The broad peak indicates the existence of microstructure, which does not exist in neutral polymer solutions. Strong correlation may exist between the microstructure and macroscopic properties of polyelectrolytes solutions.[1][2]

The broad peak in the scattering intensity curve of polyelectrolyte solutions is known to change its shape with salt concentration and pH. Recently, we surprisingly found that the peak was also strongly influenced by the applied electric field during a SAXS experiment when the polyelectrolyte is confined in a matrix (polymer gel). The peak top shifted towards high q region when a weak direct-current electric field was applied (0.3 V/cm) (Figure 1).

Since the steady movement of polyelectrolyte along the electric field can be ignored in the static scattering measurement, the peak shift in Figure 1 clearly indicates the change in the microstructure of polyelectrolytes. This phenomenon has never been reported. In this study, we planned to systematically study the influence of electric field on the microstructure of polyelectrolyte.

To investigate the influence of electric field on polyelectrolytes, we planned to performed a series of SANS experiment for a model polyelectrolyte, polystyrene sulfonate sodium (PSS, Mw = 3,000-100,000), in D2O buffer and in a fixed matrix (polyacrylamide gels) with different polymer concentration (1-6 wt%) under different electric field strength (0-10 V/cm) at r.t. All samples were prepared in a custom-made SANS cell. The electric field was applied via a high voltage DC supply system (EF-1: Electric Field, 10 kV) in Quokka.

Unfortunately, most of the experimental time allocated to this study was used to setup the DC power supply system, the special instrument alignment and the sample holder. We successfully applied electric field to one sample and tried to obtain the scattering profile. However, the neutral polymer gel, which was used as the matrix to confine polyelectrolyte polymers, was detached from the quarz glass plates shortly after we started the SANS experiment. The detachment of the polymer gel resulted from the repeatedly use of the same quarz glass plates; the surface of glass plates were chemically modified by the gelation reaction.

Thanks to the efferts by Dr. Elliot, Dr. Norman and many other staff in ANSTO to construct the special setup for electrophoresis SANS during this experiment, we established an excellent electrophoresis system in Quokka. We plan to use this system again to retry this study in the future.

Aggregation structure of thermoresponsive hydrogels consisting of a homogeneous network

S. Nakagawa (1), X. Li (1), and M. Shibayama (1)
(1) Institute for Solid State Physics, University of Tokyo

Hydrogels, which consist of water and a polymer network, are a useful material in the medical and bio-science fields. We have recently developed a new thermoresponsive hydrogel whose swelling behavior could be controlled via temperature. This hydrogel was prepared by end-linking of two prepolymer units; four-armed poly(ethylene glycol) (Tetra-PEG) and four-armed poly(ethyl glycidyl ether-co-methyl glycidyl ether) (Tetra-PEMGE). PEG was a hydrophilic polymer while PEMGE was a thermoresponsive polymer that was hydrophilic at lower temperature but hydrophobic at higher temperature. The hydrogel with the mole fraction of Tetra-PEMGE units, r_PEMGE, of 40% did neither absorb nor expell water at physiological temperature, i.e., it was practically a nonswellable hydrogel. We found by SANS measurements that more than 10 prepolymer units aggregated to form a single spherical domain, leading to significant deformation of the network. In this study, we investigated the domain structure of the hydrogels with different r_PEMGE by means of SANS to gain insight into the aggregation of thermoresponsive prepolymer units in the nonswellable hydrogel.

The hydrogel samples used in this study were prepared by mixing Tetra-PEG and Tetra-PEMGE solutions in D2O phosphate buffer. Four samples with different mole fraction of Tetra-PEMGE units, r_PEMGE, of 1, 2, 5, and 10% were prepared. SANS measurements were performed using QUOKKA at the OPAL reactor in ANSTO, Australia. The wavelength was 5 A and two configurations with the sample-to-detector distance of 1.3 and 8 m were used. The temperature of the samples was controlled by a 20-position temperature-variable sample changer.

Fig. 1 shows the SANS profiles for Gel01, Gel02, Gel05, and Gel10 at temperatures ranging from 14 °C to 60 °C. At temperatures lower than ~ 20 °C, all the samples exhibit simple scattering profiles with a slight upturn in the low-q region and a shoulder followed by a power-law decay in the high-q region. The upturn in the low-q region should be attributed to the clustering of the end-groups of Tetra-PEG and Tetra-PEMGE, which can also be observed for PEG solutions. The shoulder and a power-law decay in the high-q region are similar to the Ornstein-Zernike function for homogeneous semidilute solutions and gels. These facts indicate that the network in all four samples is homogeneous in this temperature range, aside from the clustering due to end-groups. The profiles for Gel02, Gel05, and Gel10 at temperatures higher than 20 °C contain a peak in the low-q region and a shoulder in the higher-q side. We found similar scattering profiles for the hydrogel with r_PEMGE = 40% in the previous study, where we cocluded from model fitting analyses that multiple Tetra-PEG and Tetra-PEMGE units aggregated to form spherical domains. Given the qualitative similarity of the profiles between the present and previous studies, we believe that spherical domains are formed also in Gel02, Gel05, and Gel10. Note that Gel01 does not exhibit distinct peak in all temperatures, indicating that Tetra-PEMGE units cannot aggregate into domains if the number density of Tetra-PEMGE units is too low. For Gel02, Gel05, and Gel10, the peak and shoulder can be attributed to the inter-domain (structure factor) and intra-domain (form factor) correlations, respectively. The peak position shifts to the lower-q side with decreasing r_PEMGE, indicating that the number density of the domains de-

creases and distance between two neighboring domains increases. This also affects the width of the peak; as the neighboring domains become more separated to each other, correlation of the domain position is gradually lost, leading to broadening of the peak. The shoulder becomes less discernible with decreasing r_PEMGE, indicating that either the interfacial thickness and/or polydispersity of the radius of spherical domains becomes larger as the number density of Tetra-PEMGE units decreases.

In summary. we performed a series of SANS measurements on the thermoresponsive hydrogels with different mole fractions of thermoresponsive prepolymer units r_PEMGE and found that the domain structure formed by aggregation of thermoresponsive prepolymer units depended significantly on r_PEMGE. Further detailed analyses on the obtained SANS profiles are now in progress, which will provide a comprehensive picture of the structure formation in thermoresponsive hydrogels.

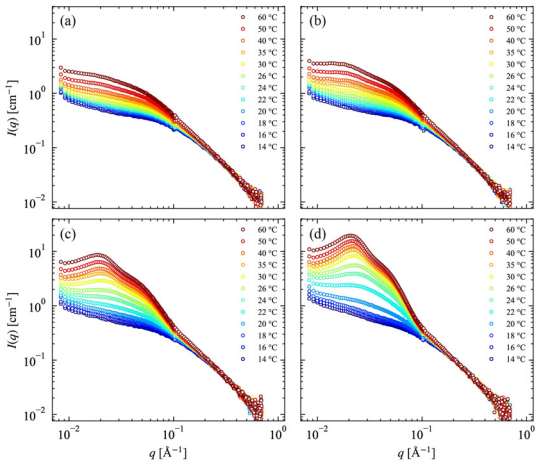

Fig. 1. Fig. 1. SANS profiles of Gel01 (a), Gel02 (b), Gel05 (c), and Gel10 (d) at different temperatures ranging from 14 to 60 °C.

Elucidation of the Mechanism of the Solvent-Dependent Switch of Helical Main-Chain Chirality of Poly(quinoxaline-2,3-diyl)s by Small Angle Neutron Scattering

Yuuya Nagata, Sota Sato, Masaaki Sugiyama
Graduate School of Engineering, Kyoto University; Department of Chemistry, The University of Tokyo; Research Reactor Institute, Kyoto University

Much interest has been focused on the screw-sense control of helical polymers because of their applications for asymmetric catalysts and chiroptical materials. Recently, we reported the synthesis of single-handed helical poly(quinoxaline-2,3-diyl)s (PQXs) bearing chiral side chains and their solvent-dependent helix inversion, which can serve as effective scaffold for chirality-switchable polymer catalysts and chiroptical materials. On the other hand, the mechanism of the solvent-dependent helix inversion of PQXs has been unclear. In this experiment, we carried out small-angle neutron scattering (SANS) experiments of solutions of PQXs for the elucidation of the mechanism of the solvent-dependent helix inversion.

A PQX bearing chiral 3-octyloxymethyl groups shows the solvent-dependent helix inversion in saturated hydrocarbons such as n-octane, isooctane, and cyclooctane. We prepared 100mer of the PQX bearing (S)-3-octyloxymethyl side chains, which was dissolved into deuterated solvents to measure the SANS patterns of these solutions. According to our preliminary experiment using circular dichroism spectroscopy, the polymer adopts left-handed helical conformation in n-octane, right-handed helical conformation in cyclooctane, and almost racemic structure in isooctane. These solutions afforded different SANS patters, reflecting the conformation of the PQX, depending the saturated hydrocarbons (Figure 1 measured in QUOKKA, ANSTO, Australia, 21/6/2016-24/6/2016). Now we are trying to determine the detailed models for each SANS patterns using computer simulations to reveal the mechanism of the solvent-dependent helix inversion of the PQX in saturated hydrocarbons.

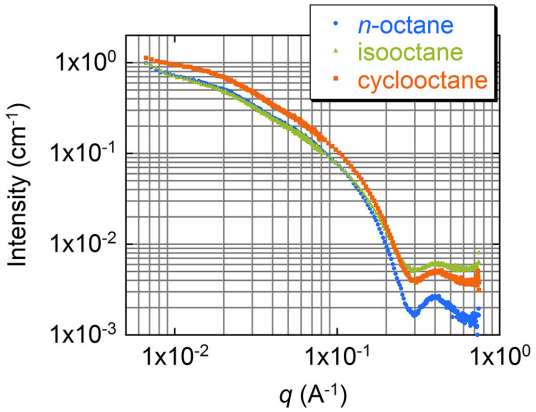

Fig. 1. SANS patterns of the PQX bearing (S)-3-octyloxymethyl side chains in n-octane, isooctane, or cyclooctane.

Thermodynamical Study on Phase Behavior of Thermo-responsive Polymer in Hydrophobic Ionic Liquids.

Kazu Hirosawa, Xiang Li, Ken Morishima, and Mitsuhiro Shibayama
The Institute for Solid State Physics

Ionic liquids (ILs) are molten salts having their melting points near room temperature. Recently, it was reported that poly(benzyl methacrylate) (PBnMA) and its derivatives show a lower critical solution temperature (LCST)-type phase separation in ILs. Interestingly, the phase separation temperature (T_c) of the thermo-responsive polymers in IL systems strongly depends on both chemical structures of the polymer and the ILs; one of the PBnMA-derivatives, PPhEtMA (see Fig. 1(a)) exhibits LCST-type phase behavior at 315 K, 391 K, and 393 K in [C_2mIm][TFSA], [C_4mIm][TFSA], and [Py_{14}][TFSA], respectively. Such a tendency indicates that the macroscopic phase behavior of the systems is controlled by microscopic molecular interactions.In the present study, we carried out small-angle neutron scattering (SANS) experiments for PPhEtMA in deuterated ILs, (1)d_8-[C_2mIm][TFSA], (2)d_{12}-[C_4mIm][TFSA], and (3)d_9-[Py_{14}][TFSA] to investigate the correlation between microscopic polymer-IL interactions and the LCST-type phase behavior. Here, in comparison with system (1), we examined the effect of (2) the side chain length and (3) the existence or absence of π-conjugated electron system in the IL cation. Fig. 2(b) shows a representative SANS profiles at elevated temperatures which are close to the cloud point. As shown, the scattering intensity at the low-q region gradually increased with temperature indicating that the excluded volume effect of polymer chains decrease with temperature. The effective Flory-Huggins interaction parameter, $\chi_{\mathrm{eff}}(T)$, was estimated by a curve fitting procedure. Furthermore, the enthalpic (χ^H_{eff}) and the entropic (χ^S_{eff}) contribution to $\chi_{\mathrm{eff}}(T)$ were obtained as an intercept and a slope of a $\chi_{\mathrm{eff}}(T)$ vs $1/T$ plot, respectively. As a result, both of χ^H_{eff} and χ^S_{eff} systematically varied with the chemical structure of the ILs. To obtain a precise interpretation to the variation of χ^H_{eff} and χ^S_{eff}, we carried out high-energy X-ray total scattering (HEXTS) experiment to investigate the microscopic solvation structure. The analysis of the obtained HEXTS data is now in progress. After completing the analysis, we will be able to understand the macroscopic phase behavior of the thermo-responsive polymer in IL systems from a viewpoint of the microscopic molecular interactions.

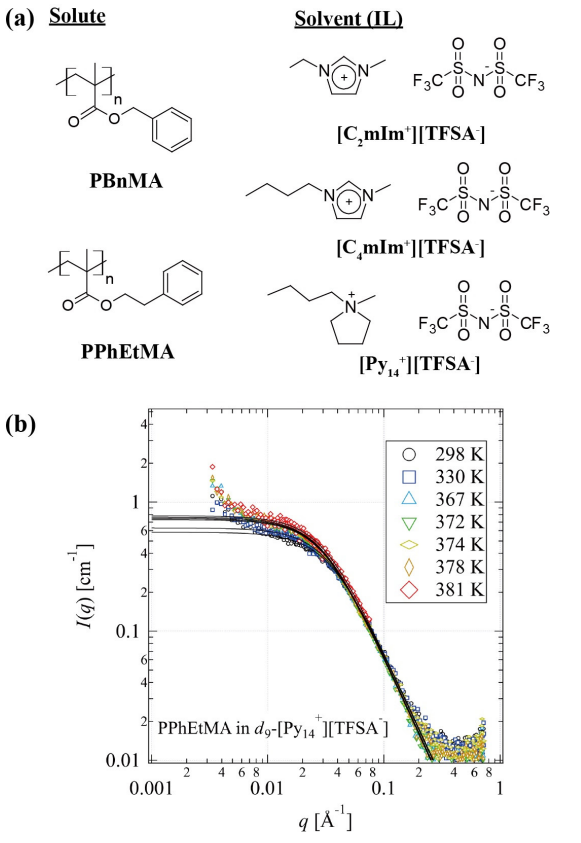

Fig. 1. (a) Chemical structures of polymers and ILs. (b) A representive SANS profiles obtained for PPhEtMA in d_9-[Py_{14}][TFSA] solution.

Others

Investigation of nanoparticles in ODS Ni-free austenitic steel

A. Kowalska-Moriˆ1,2, H. Mamiyaˆ1,
1 National Institute for Materials Science, 2 Warsaw University of Technology

Oxide dispersion strengthened (ODS) austenitic steel is a unique material, which has potential for application for future fusion power plants. Introduction of yttrium oxides (Y2O3) to the material improve irradiation resistance and high temperature strength. The nano ?particles play important role in strengthening material by pinning mobile dislocation and stabilization grain boundaries. The interfaces between the matrix and the particles act as sinks for the irradiation-induced defect. Most commercial austenitic steel contain molybdenum and very high amount of nickel which are high-activation elements. It effects in creation of undesirable, radioactive waste. Hence, we have proposed a new material nitrogen containing nickel-free ODS austenitic steel. It is considered as a material for advanced reactor technologies

The Fe-13Cr-20Mn-0.35 Y2O3 and Fe-13Cr-20Mn-0.35 Y2O3-xTi alloys was manufactured by mechanical alloying followed by spark plasma sintering. The as-milled powder was sintered in 950 C or 1000 C for 5 or 15 min. To study the thermal stability of nanoparticles, we have annealed one of the samples (sample sintred in 1000 C for 5) for 1h in temperatures range form 700 C to 1000 C.

We carried out small-angle neutron scattering (SANS) using QUOKKA on assistance of ISSP. We used neutrons with the wavelength 2.95 Å and q-range from 6 x 10ˆ-4 Aˆ-1 to 0.7 Aˆ-1 with standard and focusing lens optics The measurements were held in the ambient temperature with non-polarized neutron. Source aperture to sample aperture distance was 3, 12 and 20 m and focusing lens optics (L1=12m L2=1p3m offset_apx5). The measured data was corrected by using the results of the glassy carbon and thickness and analyzed by Irena software using Size Distribution. To obtain information about size, number and chemcial composition of nanoparticles, we have applied the alloy contrast variation analysis (ACV), combining USAXS and SANS data. The ACV method is based on the difference of X-ray and neutron scattering length of each element, which is described as a ratio of intensity between SANS and SAXS.

In low-q regoin, we observed clear humps in all samples. Increase of sintering temperature causes humps shifting to lower q-value. Samples sintered in 950 C have a mean radius around 200 A. In 1000 C occurred particles growth up to 270 A for samples sintered in 5 min and 380 for the samples sintered for 15 minutes. The biggest nanoparticles were obtained in samples with 0.1% Ti sintered in 950 C for 15 min.

Next, we have considered the SANS and USAXS curves in the ACV analysis. The analysis indicates presence of two population of Y2O3, ε-martensite and MnO nanoparticles, what is correct according to XRD, TEM and EDS results. The presence of very fine Y2O3, radius round with 20 A is suggested, it has occurred re-precipitation of dissolved Y2O3 during mechanical alloying. The results of ACV analysis of annealed samples show increase of volume distribution of the finest Y2O3 after annealing in 800 C. The nanoparticles are stable up to 900 C. In 1000 C growth of all nanoparticles occurred, and the third population of coarse Y2O3 appeared.